Cell

Insular cortex neurons encode and retrieve specific immune responses

Graphical abstract

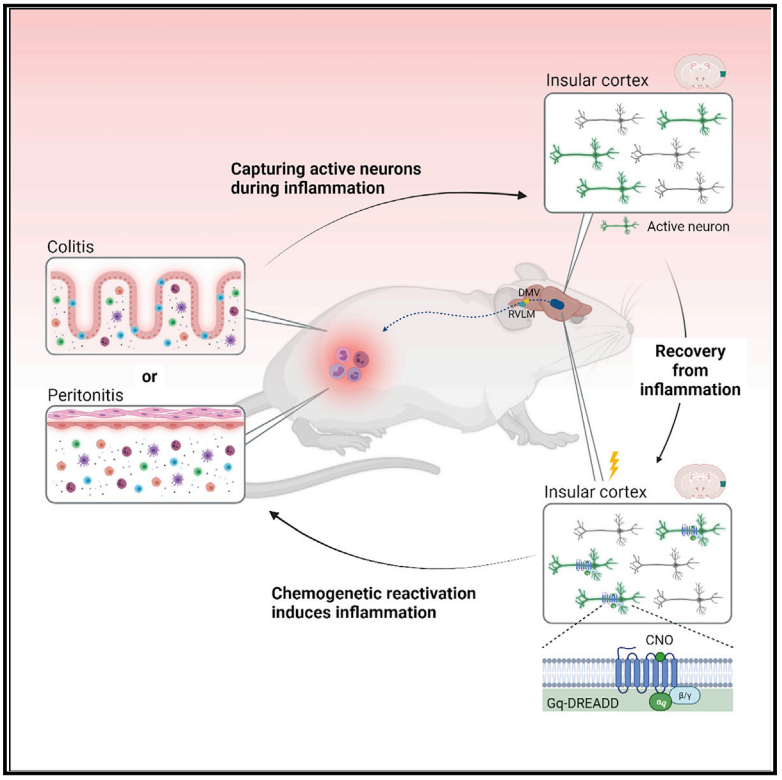

Authors

Tamar Koren, Re'ee Yifa, Mariam Amer, ..., Oren Kobiler, Kobi Rosenblum, Asya Rolls

Correspondence

rolls@technion.ac.il

In brief

Neuronal ensembles in the mouse insular cortex activated during distinct inflammatory conditions are capable of retrieving or suppressing the associated peripheral immunological responses.

Highlights

- Neuronal ensembles in the InsCtx are activated during peripheral inflammation
- Reactivation of these neurons is sufficient to retrieve peripheral inflammation
- These InsCtx neurons project to autonomic nervous system control sites (DMV, RVLM)
- Inhibition of the InsCtx alleviates inflammation during DSS-induced colitis

Koren et al., 2021, Cell *184*, 5902–5915
November 24, 2021
https://doi.org/10.1016/j.cell.2021.10.013

CellPress

CellPress

Cell

Article

Insular cortex neurons encode and retrieve specific immune responses

Tamar Koren,[1,2] Re'ee Yifa,[1,2] Mariam Amer,[1,2] Maria Krot,[1,2] Nadia Boshnak,[1,2] Tamar L. Ben-Shaanan,[3,4] Hilla Azulay-Debby,[1,2] Itay Zalayat,[1,2] Eden Avishai,[1,2] Haitham Hajjo,[1,2] Maya Schiller,[1,2] Hedva Haykin,[1,2] Ben Korin,[5] Dorit Farfara,[1,2] Fahed Hakim,[6,7] Oren Kobiler,[8] Kobi Rosenblum,[9,10] and Asya Rolls[1,2,11,*]

[1]Department of Immunology, Rappaport Faculty of Medicine, Technion - Israel Institute of Technology, Haifa, Israel
[2]Department of Neuroscience, Rappaport Faculty of Medicine, Technion - Israel Institute of Technology, Haifa, Israel
[3]Department of Microbiology and Immunology, University of California, San Francisco, San Francisco, CA, USA
[4]Howard Hughes Medical Institute, University of California, San Francisco, San Francisco, CA, USA
[5]Department of Research Biology, Genentech, South San Francisco, CA, USA
[6]Pediatric Pulmonary Unit, Rambam Health Care Campus, Haifa, Israel
[7]Cancer Research Center, EMMS Hospital, Nazareth, Israel
[8]Sackler School of Medicine, Tel Aviv University, Israel
[9]Sagol Department of Neurobiology, University of Haifa, Haifa, Israel
[10]Center for Gene Manipulation in the Brain, University of Haifa, Haifa, Israel
[11]Lead contact
*Correspondence: rolls@technion.ac.il
https://doi.org/10.1016/j.cell.2021.10.013

SUMMARY

Increasing evidence indicates that the brain regulates peripheral immunity, yet whether and how the brain represents the state of the immune system remains unclear. Here, we show that the brain's insular cortex (InsCtx) stores immune-related information. Using activity-dependent cell labeling in mice (*Fos*^{TRAP}), we captured neuronal ensembles in the InsCtx that were active under two different inflammatory conditions (dextran sulfate sodium [DSS]-induced colitis and zymosan-induced peritonitis). Chemogenetic reactivation of these neuronal ensembles was sufficient to broadly retrieve the inflammatory state under which these neurons were captured. Thus, we show that the brain can store and retrieve specific immune responses, extending the classical concept of immunological memory to neuronal representations of inflammatory information.

INTRODUCTION

Accumulating data indicate that the brain can affect immunity, as evidenced, for example, by the effects of stress (Chovatiya and Medzhitov, 2014; Dhabhar, 2014; Silberman et al., 2003), stroke (McDonald et al., 2010; Prass et al., 2003; Wong et al., 2011), and reward system activity (Ben-Shaanan et al., 2016, 2018) on the peripheral immune system. However, our understanding of this neuroimmune interaction is still limited. Importantly, we do not know how the brain evaluates and represents the state of the immune system.

As a central regulator, it is likely that the brain receives feedback from any system it controls and, by extension, forms representations of the immune system. This concept is supported by several lines of evidence. First, anatomically, the brain receives immune-related information via sensory inputs from peripheral immune organs, such as the spleen and lymph nodes (Dantzer, 2018; Goehler et al., 2000; Pavlov and Tracey, 2017). Second, the brain responds to peripheral immune challenges. For example, neuroimaging studies identified increased activation of specific brain regions (e.g., the amygdala, hypothalamus, brainstem, thalamus, and insular cortex [InsCtx]) during peripheral inflammation (Harrison et al., 2009; Sergeeva et al., 2015). Finally, the immune system has been shown to respond to immune conditioning by associating a specific immune response (e.g., immune suppression) with an external cue (e.g., saccharin water), such that presentation of the cue alone can elicit the immune response (Ader and Cohen, 1975; Hadamitzky et al., 2020). This suggests that the brain encodes immune-related information (Cohen et al., 1994). Furthermore, lesion studies identified specific brain regions required for immune conditioning, notably, the InsCtx (Ramírez-Amaya et al., 1996, 1998). However, the existence of such immune representations in the brain was never directly demonstrated.

The current study was designed to test the existence of immune-related information in the brain and determine its relevance to immune regulation. We hypothesized that the InsCtx, specifically the posterior InsCtx, is especially suited to contain such a representation of the immune system. This region is considered the primary cortical site of interoception (i.e., the sensing of the body's physiological state; Craig, 2003; Gogolla, 2017) and integrates information regarding bodily sensations, such as pain, hunger, and visceral signals (Craig, 2002). Although immune-related information is not a conventional aspect of

interoception, it could provide an important indication of the organism's physiological status (Kipnis, 2018) and thus may also be processed in the posterior InsCtx. Moreover, the InsCtx is well positioned to gather immune-related information, as it receives input from peripheral neurons that respond to immune signals (Goehler et al., 2000; Reardon et al., 2018; Thayer and Sternberg, 2009). Accordingly, studies have shown that immune challenges impact insular activity (Critchley and Harrison, 2013; Doenlen et al., 2011). Finally, as previously mentioned, lesion studies have shown that the InsCtx is essential for immune conditioning (Pacheco-López et al., 2005; Ramírez-Amaya and Bermúdez-Rattoni, 1999), further supporting the hypothesis that this brain region can form immune-related representations.

RESULTS

Increased neuronal activity in the InsCtx during DSS-induced colitis

To capture neurons that were active during a peripheral immune challenge, we used transgenic targeted-recombination-in-active-populations (TRAP) mice (DeNardo et al., 2019; Guenthner et al., 2013) (Figure 1A). These mice express iCreER^{T2} under the control of an activity-dependent c-Fos promoter (*Fos*^{TRAP} mice), which serves as an indicator of neuronal activity. In the presence of tamoxifen (TM), active neurons drive Cre-dependent recombination to induce the expression of an effector gene (e.g., fluorescent reporter). For the immune challenge, we chose a model of colon inflammation (colitis). Emerging experimental and epidemiological data established the significance of the gut-brain axis in gastrointestinal (GI) inflammatory conditions (Fung et al., 2017; Powell et al., 2017; Veiga-Fernandes and Mucida, 2016; Willemze et al., 2015). The InsCtx receives information through the brainstem and thalamus from this highly innervated and immunologically active visceral organ (Han et al., 2018; Hobday et al., 2001; Kaelberer et al., 2018; Mayer, 2011). Thus, we used a model of inflammatory bowel disease (IBD), dextran sulfate sodium (DSS)-induced colitis, to capture its potential representation in the InsCtx.

We crossed the TRAP mice with a Cre-dependent tdTomato reporter line, *Ai14D* (Madisen et al., 2010), to visualize the active cells. Mice were injected with TM (inducing Cre recombination and as a result, tdTomato expression) 48h after initiation of the DSS treatment (DSS^{+} group). As controls, we used another group of TRAP-tdTomato mice that were injected with TM at the same time but did not receive DSS (DSS^{-} group; Figure 1B). This group allowed us to compare between inflammation-related activity in the brain, and brain activity during healthy homeostasis. Automated survey of whole brains revealed increased tdTomato expression (indicative of neuronal activity) in several brain areas (Table S1), including the thalamus (receives sensory and visceral information), the paraventricular hypothalamic (PVH) nuclei (involved in physiological homeostasis and stress), the central amygdala (CeA; fear and memory formation), the anterior cingulate cortex (ACC), the supplementary somatosensory cortex (S2; parts of the pain matrix), and the InsCtx ($p < 0.0001$; Figures 1C and 1D). Thus, consistent with previous studies (Belevych et al., 2010; Buller and Day, 2002; Hanken et al., 2014; Harrison et al., 2009; Zhang et al., 2000), the brain, including the InsCtx, responds to peripheral immune challenge.

Based on this analysis and our prediction of the InsCtx functioning as an interoceptive site that receives immune-related information, we chose to focus on this area. Moreover, since the InsCtx exhibits some functional lateralization, we focused on the right InsCtx, which is more dominantly associated with sympathetic afferent innervation and visceral information processing (Montalbano and Shane Tubbs, 2018). To target the TRAPing to this brain region and limit the labeling to neuronal populations, we used a viral vector instead of the TRAP-tdTomato reporter mice. The viral vector encoded the mCherry fluorescent reporter, expressed in a Cre-dependent manner under a neuronal-specific promoter, synapsin, and was stereotactically injected to the right posterior InsCtx of TRAP mice. To capture active neurons during colitis, we injected the mice with TM 48 h after initiation of the DSS treatment (Figure 1E). Most of the labeled cells (Figure 1F) were neurons rather than astrocytes or microglia (Figure 1G). More specifically, as determined by *in situ* hybridization, 71% of the TRAPed cells were glutamatergic, and 20% were GABAergic (Figure 1H). Thus, DSS-induced colitis is associated with increased activation of neurons in the InsCtx. However, such correlative findings are not sufficient to demonstrate that these neurons indeed encode immunologically relevant information.

Reactivation of InsCtx neuronal ensembles captured during colitis recapitulates an inflammatory state in the colon

To directly address this question, we reactivated the TRAPed neurons and evaluated their effects on the immune response. For the neuronal reactivation, we co-expressed a stimulatory DREADD (designer receptors exclusively activated by designer drugs; Gq) in the captured neurons. DREADDs are mutated muscarinic G-protein-coupled receptors (GPCRs) activated by a synthetic ligand, clozapine *N*-oxide (CNO). Thus, CNO application enables the reactivation of the captured neurons at will. The control group was injected with a virus encoding the mCherry fluorescent reporter but lacking the DREADD-coding sequence (sham; Figure 2A). This sham group allowed us to control for the surgical procedure, viral vector expression, amount of DSS water consumed (Figure S1A), and application of CNO. As in the previous experiment, we injected TM 48 h following initiation of the DSS treatment to capture the active InsCtx neurons and enable their expression of both Gq-DREADDs and a fluorescent reporter. After 4 weeks of recovery, we reactivated the captured InsCtx neuronal ensembles (by CNO injection; validated by c-Fos staining; Figures 2B, 2C, and S1B–S1D) and evaluated their effects on the peripheral immune response (Figure S1). We also determined the tissue histopathology and permeability state (Figures S1E and S1F), weight loss (Figure S1G), histology severity score (Figures 2D and S1H), and inflammation (Figures 2E–2P and S1I–S1V). Even in the absence of an additional immune challenge, neuronal reactivation resulted in heightened immune activity in the colon of the Gq mice, in agreement with the changes evident during the initial or a repeated DSS treatment (Figures 2E–2P and S2). There was a significant increase in the percentage of leukocytes present in the mucosal layer of the colon, including the intraepithelial lymphocytes (IELs) and

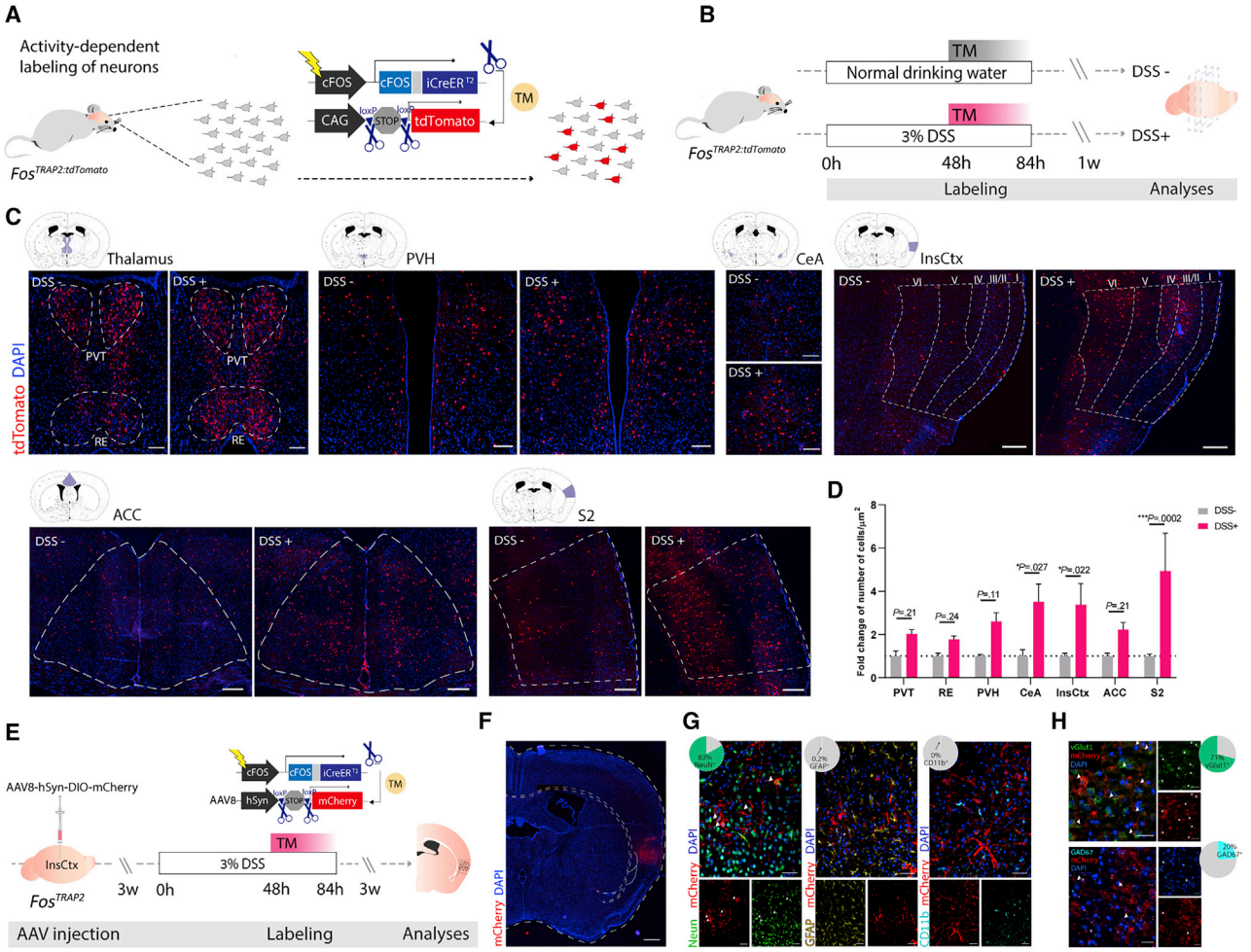

Figure 1. Activity-dependent labeling of neurons during DSS-induced colitis in the mouse InsCtx

(A) Activity-dependent neuronal labeling in *Fos*$^{TRAP2:tdTomato}$ mice. iCreER^{T2} is expressed in activated neurons, indicated here by c-Fos expression. The administration of TM allows iCreER^{T2} recombination to occur only in active neurons. Thus, only neurons that are active while TM is present at sufficient levels (~24–36 h following administration) will express the Cre-dependent fluorescent reporter (tdTomato).

(B) Fluorescently labeling neurons active during DSS-induced colitis (DSS+) or a normal drinking water regime (DSS-) in *Fos*$^{TRAP2:tdTomato}$ mice.

(C) tdTomato expression in different brain regions of both experimental groups: thalamus (paraventricular nucleus of the thalamus, PVT; nucleus of reuniens, RE), paraventricular nucleus of the hypothalamus (PVH), central amygdala (CeA), right insular cortex (InsCtx), anterior cingulate cortex (ACC), and supplementary somatosensory cortex (S2). Scale bars: 50 µm (Thalamus, PVH, CeA), 100 µm (InsCtx), 200 µm (ACC, S2).

(D) Quantification of tdTomato-TRAPed neurons in each of the presented brain regions. Two-way ANOVA and Benjamini, Krieger, and Yekutieli Multiple comparisons (n = 4–7, 3–6).

(E) Fluorescence labeling of neurons active during DSS-induced colitis in the InsCtx.

(F) Expression of the injected Cre-dependent fluorescent marker (mCherry, in red) in the InsCtx, 3 weeks following TM administration. Scale bar: 250 µm.

(G) Representative brain micrographs showing immunofluorescence (IF) staining of the labeled cells in the InsCtx (mCherry, red) co-stained for neuronal (NeuN, green; n = 6), astrocytic (GFAP, yellow; n = 5), and microglial (CD11b, cyan; n = 6) markers. Scale bars: 50 µm.

(H) Representative images of single-molecule fluorescence *in situ* hybridization (smFISH) staining in the InsCtx, demonstrating the identity of 71% ± 1.45 SEM labeled cells as glutamatergic (vGlut1$^+$, upper micrograph) and 20% ± 3.7 SEM as GABAergic (GAD67$^+$, lower micrograph). n = 4. Scale bars: 25 µm. White arrows indicate double-positive cells for mCherry and the added cellular marker. Pie charts indicate percentages of double stained neurons out of all mCherry$^+$ cells, for each marker. AAV, adeno-associated virus; lightning symbol, neuronal activity; TM, Tamoxifen; DSS, dextran sulfate sodium. Data represent two independent repeats. See also Table S1.

leukocytes within the lamina propria (LP; Figures 2E and S1M). Activated γδ T cells increased in the IEL and decreased in the LP in the Gq group compared to the sham-treated mice (Figures 2F, 2G, and S1N), a characteristic trend that was previously demonstrated for γδ T cells during intestinal infection (Hoytema van Konijnenburg et al., 2017). Moreover, we found higher proportions of activated CD4$^+$ T cells (Figures 2H, 2I, S1O, and S1P) and an increase in the activation of CD8$^+$ T cells (Figures 2J, 2K, and S1Q–S1S). Similarly, we observed an increase in the percentage of a specific dendritic cell (DC) subset

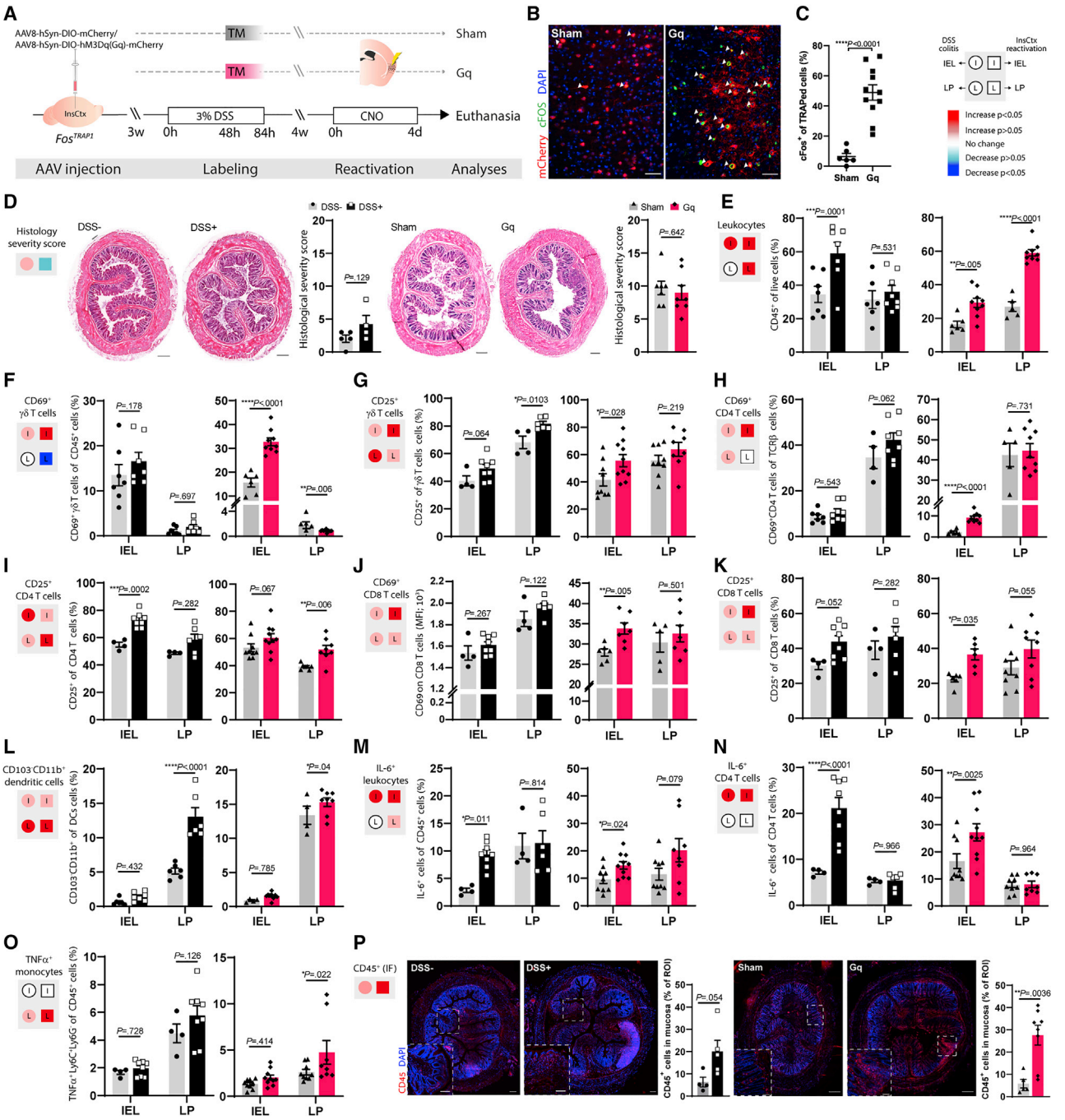

Figure 2. Reactivation of InsCtx neuronal ensembles captured during colitis recapitulates an inflammatory state in the colon

(A) Schematic representation of TRAPing InsCtx neurons during DSS-induced colitis and their reactivation upon recovery.

(B) Representative micrographs of InsCtx showing both sham viral vector- (left, mCherry) and Gq-DREADD- (right, mCherry) expressing neurons, stained for c-Fos (green) 90 min following the last CNO administration. Scale bar: 100 μm.

(C) Quantification of c-Fos-expressing neurons percentages out of mCherry-expressing (TRAPed) neurons in the InsCtx. Student's *t*-test (n = 6, 11). Top right: legends indicating the trend and significance levels in the comparison between the original DSS effects and the effects induced by Gq activation on the colon, provided on the left of (D–P).

(D) Representative images and histological severity score of colons obtained from DSS+ mice (receiving 3% DSS in their drinking water for 84 h) and their non-inflamed DSS- controls (n = 5, 4; left) and from Gq-expressing mice and their Sham controls (n = 7, 8; right) following 4 days of daily CNO injections. Scale bar: 200 μm. Student's *t*-test.

(legend continued on next page)

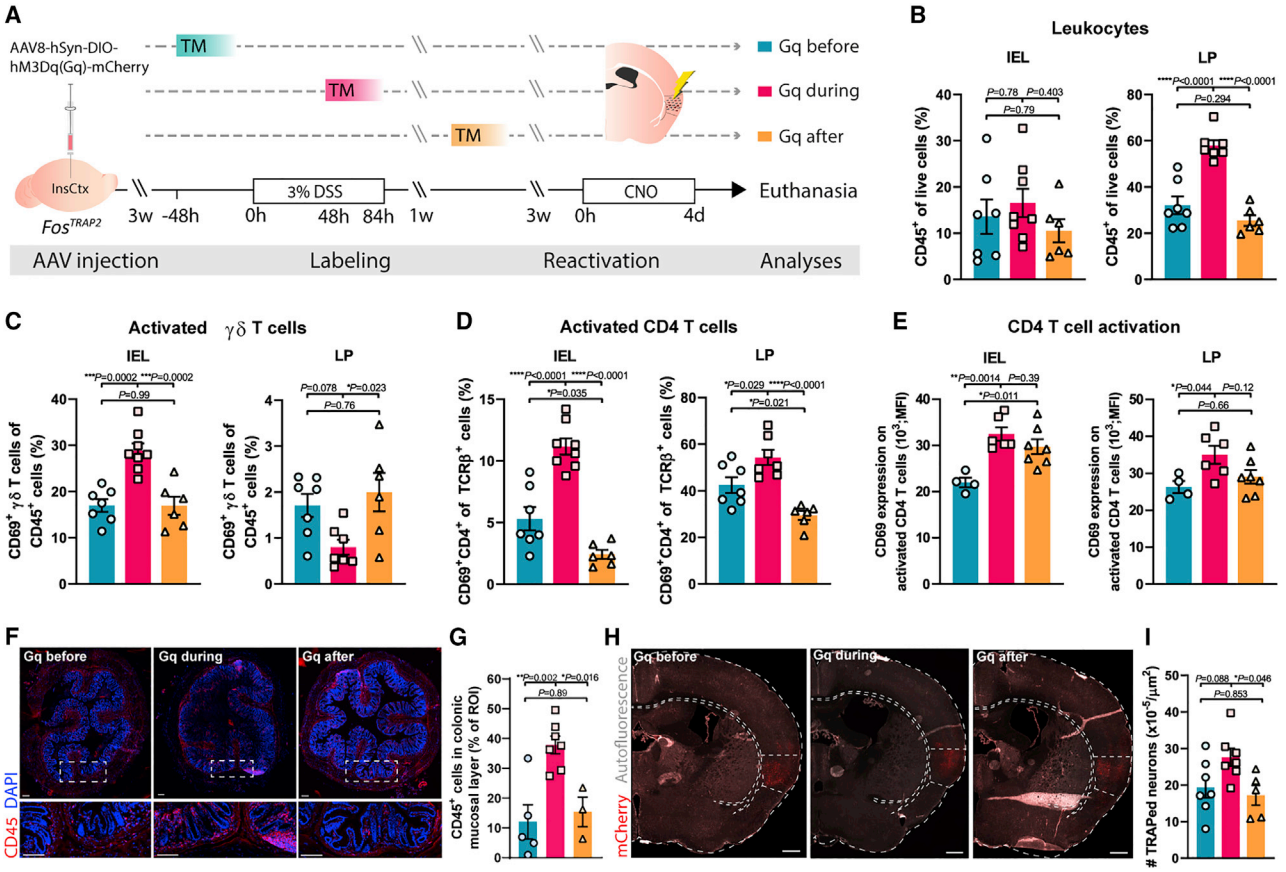

Figure 3. Reactivation of neuronal ensembles captured at different stages of DSS-induced colitis generates different immune responses in the colon

(A) Schematic representation of TRAPing InsCtx neurons via different timings of TM injections, relative to DSS treatment, and their reactivation upon recovery.

(B–E) Graphs derived from flow cytometry analysis showing percentages of (B) leukocytes, (C) activated γδ T cells, (D) activated CD4$^+$ T cells, and (E) CD69 expression (MFI) on CD4$^+$ T cells in the mucosal layer of the colon (IEL, LP) in all three Gq groups.

(F) Representative composite micrographs of colon tissue (n = 5, 7, 3), IF-stained for CD45 (red) and DAPI (blue). Scale bars: 50 μm.

(G) Quantification of CD45$^+$ cells in the IF-stained colon sections.

(H) Representative composite micrographs showing the expression of the injected Cre-dependent DREADD (mCherry, in red) in the InsCtx of all 3 experimental groups (n = 7, 7, 5). Scale bar: 250 μm.

(I) Quantification of DREADD-expressing neurons in the InsCtx of all 3 experimental groups. One-way ANOVA and Tukey's multiple comparisons test (in B–E, G, nd I).

In all bar graphs, data from individual mice are shown, and values are represented as mean ± SEM. InsCtx, Insular cortex; TM, Tamoxifen; DSS, dextran sulfate sodium; CNO, clozapine-*N*-oxide; IEL, intraepithelial lymphocytes; LP, lamina propria; MFI, median fluorescence intensity. Data represent two independent repeats. See also Figure S3.

(CD103$^-$CD11b$^+$) in the LP, known to induce specific T cell activation in the gut (Annacker et al., 2005; Liang et al., 2016) (Figures 2L and S1T). Intracellular analysis revealed an increase in the percentage of interleukin-6 (IL-6)-expressing IEL CD4 T cells (Figures 2M, 2N, and S1U) and tumor necrosis factor α (TNF-α)-expressing monocytes (in the LP; Figures 2O and S1V). These changes were also supported by all-tissue colon analysis indicating elevated TNF-α, IL-6, and IL-17 levels in the Gq group, with no significant change in the levels of the anti-inflammatory cytokine IL-10 (Figure S1W). The increase in

(E–O) Graphs derived from flow cytometry analysis showing percentages of (E) leukocytes, (F–G) activated γδ T cells, (H–I) activated CD4$^+$ T cells, (J–K) CD69 expression (MFI) on CD8$^+$ T cells and percentages of CD25$^+$ CD8 T cells, (L) percentages of CD103$^-$CD11b$^+$ DCs, (M) IL-6$^+$ leukocytes, (N) IL-6$^+$ CD4 T cells and (O) TNFα$^+$ monocytes in the colonic mucosal layer (IEL, LP) of DSS+ mice and their non-inflamed controls (left) and Gq mice relative to their sham controls following neuronal reactivation (right). Student's t-tests. (P) Representative composite micrographs of colon tissue from each experimental group, IF-stained for CD45 (red) and DAPI (blue) and its quantification (Student's t-test). Scale bars: 100 μm (whole section), 50 μm (partial section).

In all bar graphs, data from individual mice are shown and values are represented as mean ± SEM. InsCtx, insular cortex; TM, Tamoxifen; DSS, dextran sulfate sodium; lightning symbol, neuronal activity; CNO, clozapine *N*-oxide; IEL, intraepithelial lymphocytes; LP, lamina propria; MFI, median fluorescence intensity; DCs, dendritic cells. Data represent two independent repeats for each experimental design. See also Figures S1 and S2.

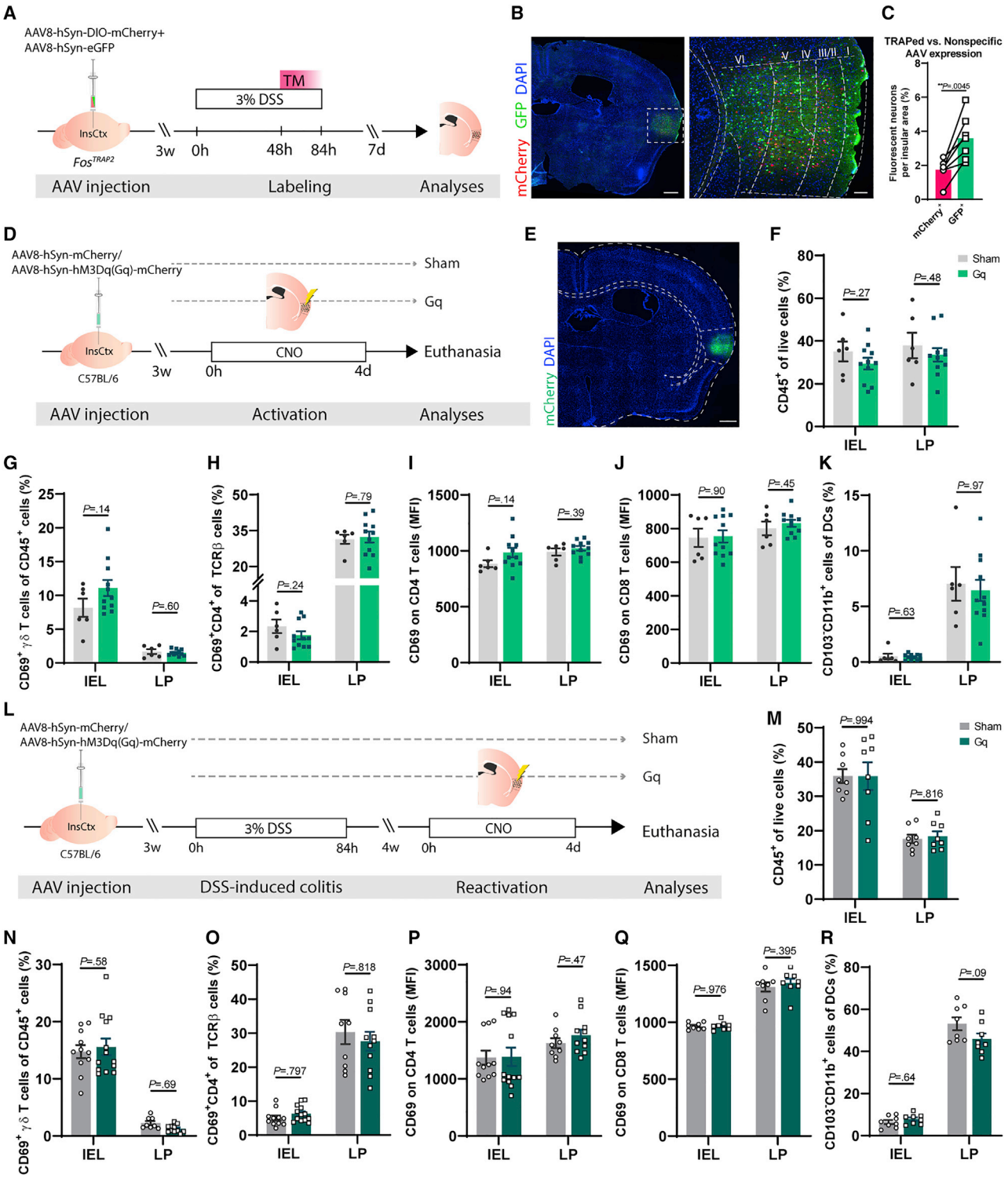

Figure 4. Nonspecific activation of the InsCtx elicits no apparent cellular immune response in the colon

(A) Fluorescent labeling of neurons in both a Cre-dependent (mCherry) and Cre-independent (GFP) manner in *Fos*^{TRAP2} mice.

(B) Representative composite imaging showing the expression of the injected fluorescent markers in the InsCtx, 7 days following TM administration. Scale bars: 250 μm (left), 100 μm (right).

(C) Quantification of activity-dependent and nonspecific labeled neurons (mCherry and GFP, respectively) in the InsCtx. Lines are connecting values of individual mice. Paired *t*-test; $n = 7$.

(legend continued on next page)

leukocyte abundance was further supported by the immunofluorescence (IF) analysis of the colon (Figure 2P). Moreover, these brain-induced effects were limited to the GI tract, as we did not detect any significant changes in immune cell populations in the peripheral blood or the mesenteric lymph nodes (mLNs) (Figure S1X). Nevertheless, some of the inflammatory effects induced by the neuronal reactivation were different (in magnitude or direction) from the response directly induced by the initial DSS administration, such as the changes observed in γδ T cells and the total percentage of leukocytes in the LP (Figures 2F and 2E, respectively). Other effects, such as an increase in mucosal granulocytes during DSS-induced colitis, were not recapitulated by InsCtx reactivation (Figure S1Y). Altogether, these observations suggest that the brain can reactivate previously acquired immune-related information. Nevertheless, the differences between these responses (original and reactivated) highlight the potential limitations of our experimental paradigm, the complexity of such brain representations, and interactions with the peripheral tissue.

Since the controls we used thus far expressed only the fluorescent reporter, CNO application did not induce any neuronal activation in this group, potentially disputing the hypothesis that the observed effects are specific to TRAPed neurons. To test whether specific neuronal ensembles can differentially affect the colon immune response, we induced neuronal reactivation in all experimental groups, but varied the immunological context at which these neurons were TRAPed. Thus, mice expressing Gq were injected with TM before, during, or after DSS (Gq before, Gq during, and Gq after, respectively). All three groups were subjected to the same experimental procedures (i.e., the same viral vector and DSS treatment) and, due to ongoing baseline activity, were all expected to TRAP neurons in the InsCtx. Upon recovery, we reactivated the captured neuronal populations, and evaluated the effects on the immune state in their colons (Figures 3A and S3).

Although all groups expressed the Gq-DREADD, only the Gq-during group showed a significant increase in the inflammatory response in the colon (Figures 3B–3G and S3C–S3F). The percentage of activated γδ T cells in the IEL population increased, while activated γδ T cells in the LP decreased (Figures 3C and S3D). Percentage of activated $CD4^+$ T cells ($CD69^+CD4^+$) increased in IELs and LP (Figures 3D and S3E), as well as their expression of the activation marker CD69 (Figures 3E and S3F). As in the previous experiment (Figure 2), the increase in LP leukocyte abundance was further supported by the IF analysis of the colon (Figure 3F and 3G). Hence, only InsCtx neurons captured during the original inflammation could induce colon inflammation.

However, the difference in the immunological outcome among the three experimental groups could be due to the number of activated neurons (Figures 3H and 3I) rather than the specific information they encode. Therefore, we expressed DREADDs in a Cre-independent manner, targeting approximately twice (2.06-fold ± 0.42-fold; $p = 0.0045$) the number of neurons in the same region in the InsCtx (Figures 4A–4E). This robust yet general activation did not induce an inflammatory response in the colon (Figures 4F–4K). Moreover, even when we repeated the nonspecific activation paradigm in mice that were previously exposed to DSS (Figure 4L), we could not detect any significant immune effect in the colon following the nonspecific InsCtx activation (Figures 4M–4R and S4). These observations further support the specificity of the information encoded by the brain and their causal effect on inducing peripheral inflammation.

Reactivation of neuronal ensembles captured during peritonitis induces immune activation, specifically in the peritoneum

To examine the nature of the immune information encoded by neuronal ensembles in the InsCtx, we added a different immune challenge, zymosan-induced peritonitis (ZIP). This well-defined inflammatory process affects another visceral area (the peritoneum), and it is immunologically distinct from the DSS-induced colitis. As in the previous experiments, Fos^{TRAP} mice were injected with the Gq-DREADD or a sham viral vector to their InsCtx. One Gq group received TM before ZIP (Gq before), while a second Gq group (Gq during) and the sham viral vector-expressing group (sham) were injected with TM during ZIP (Figure 5A). In contrast to the DSS-induced colitis, there was no difference in the number of the TRAPed neurons captured during ZIP compared to their controls (Figures 5B and 5C), possibly due to the more acute nature of this model. Following recovery, all groups were injected with CNO to induce neuronal reactivation.

As in the DSS paradigm, the observed immunological changes in the ZIP model were reminiscent of the inflammatory response directly induced by zymosan administration (Figures 5D–5O and S5). For example, the percentage of peritoneal monocytes, granulocytes, Toll-like receptor 4 ($TLR4^+$), and interferon-γ ($IFN\text{-}\gamma^+$) leukocytes (Figures 5D–5H) was increased in the Gq-during

(D) Schematic representation of viral vector expression in InsCtx neurons in a Cre-independent manner and their reactivation in C57BL/6 WT mice.
(E) Representative fluorescence microscopy imaging (composite) showing the expression of the injected DREADD (mCherry, in green) in the InsCtx. Scale bar: 250 μm.
(F–K) Graphs derived from flow cytometry analysis showing percentages of (F) leukocytes, (G) activated γδ T cells, (H) activated $CD4^+$ T cells, (I) CD69 expression (MFI) on $CD4^+$ and (J) $CD8^+$ T cells, and (K) percentages of $CD103^-CD11b^+$ DCs in the mucosal layer of the colon (IEL, LP) of Gq mice relative to their sham viral vector controls following neuronal activation. Student's *t*-test.
(L) The viral vector was expressed in InsCtx neurons in a Cre-independent manner in C57BL/6 WT mice. Three weeks after stereotactic injections, all mice received 3% DSS in their drinking water, followed by 4 days of daily CNO injections 4 weeks later.
(M–R) Graphs derived from flow cytometry analysis showing percentages of (M) leukocytes, (N) activated γδ T cells, (O) activated $CD4^+$ T cells, (P) CD69 expression (MFI) on $CD4^+$ and (Q) $CD8^+$ T cells, and (R) percentages of $CD103^-CD11b^+$ DCs in the mucosal layer of the colon (IEL, LP) of Gq mice relative to their sham viral vector controls following neuronal reactivation. Student's *t*-test.
In all graphs, data from individual mice are shown, and values are represented as mean ± SEM. InsCtx, Insular cortex; TM, Tamoxifen; DSS, dextran sulfate sodium; CNO, clozapine-*N*-oxide; IEL, intraepithelial lymphocytes; LP, lamina propria; MFI, median fluorescence intensity; DCs, dendritic cells. Data represent two independent repeats. See also Figures S4.

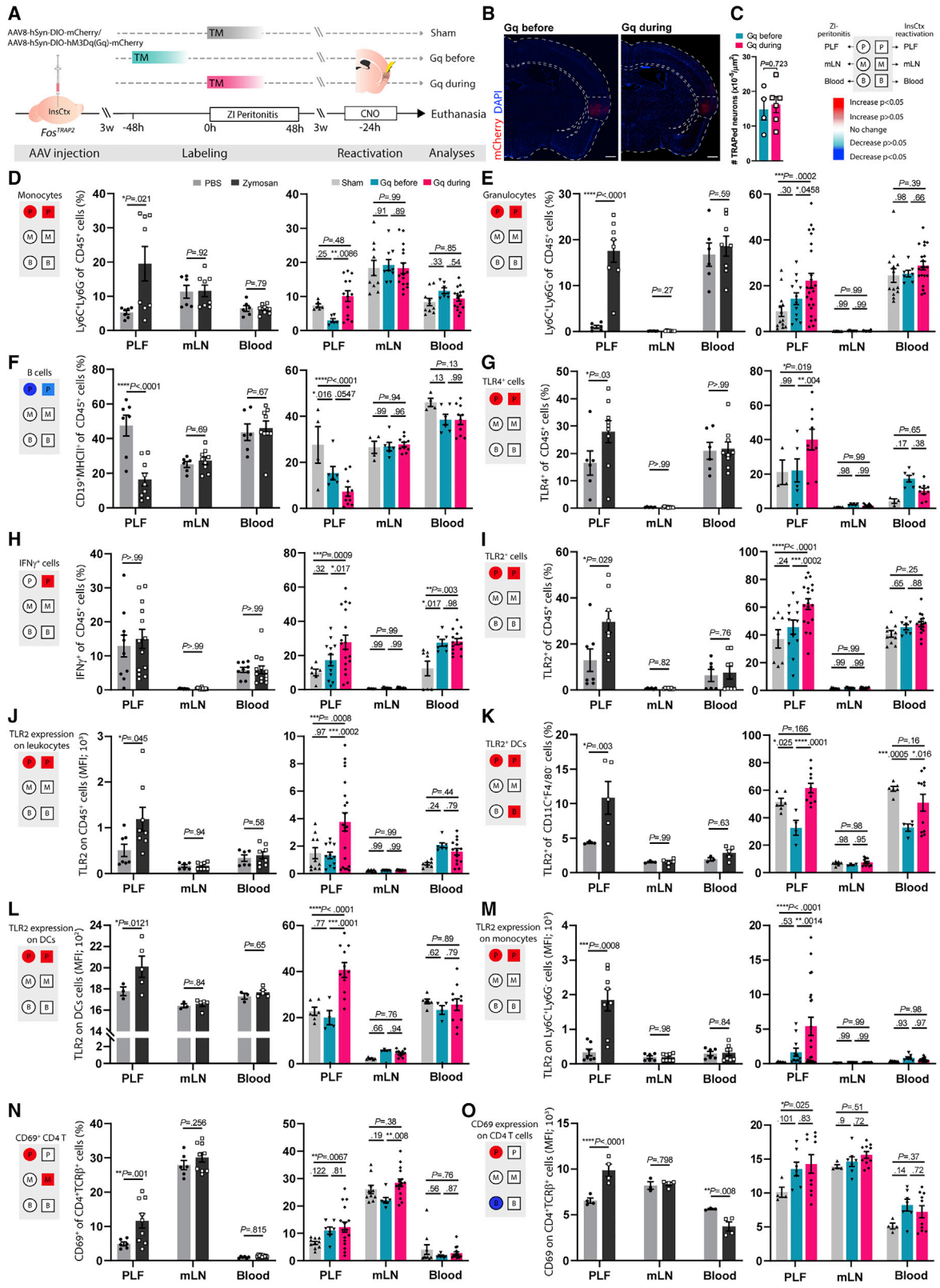

(legend on next page)

group. Similarly, expression of TLR2, which recognizes zymosan, was significantly increased on most peritoneal leukocytes in the Gq-during group (Figures 5I–5M and S5E). Moreover, we found a significant increase in the levels of the cytokines TNF-α and IL-17 in the peritoneal lavage fluid (PLF) of the Gq-during group, while no significant changes were observed in IL-6 and IL-10 concentrations (Figure S5F). As in the DSS model, some of the immune effects evident during the original inflammation were not recapitulated in the reactivation paradigm (Figures 5N–5O). Importantly, the effects induced by neurons TRAPed during ZIP were distinct from the effects detected in the DSS model (Figures 2E–2O), although in both models, we could not fully allocate the source of all elevated cytokine levels to a specific immune cell subset (Figures S5G–S5L), suggesting that other tissue cells may contribute to this phenomenon.

Importantly, the information encoded in the InsCtx also included anatomical information, since reactivation of neuronal ensembles captured during ZIP were specific to the peritoneum. We did not observe any changes in immune parameters in the colon (Figures S5M–S5R) or robust effects in the mLNs or blood (Figures 5D–5O). These results demonstrate that even without an additional immune challenge, the immune-related information encoded in the InsCtx is sufficient to induce anatomically defined, specific peripheral immune reactions.

As in the DSS-induced colitis experiment, general activation of the InsCtx, using TRAP-independent Gq expression (Figure S6A), did not induce the effects observed in the peritoneum (Figures S6C–S6J). However, in this model, when we added previous peritoneal exposure to zymosan (Figure S6B**)**, the nonspecific activation of the InsCtx recapitulated some of the immune effects that were detected in the original peritonitis, mainly the increase in TLR2 levels (Figures S6G–S6I). One possibility is that the nonspecific activation also reactivated some of the neurons that were also active during the original inflammation.

In the ''classical memory'', the neurons integrated into ensembles can vary over days and even hours (Hyman et al., 2012; Mankin et al., 2012; Sweis et al., 2021; Ziv et al., 2013). Therefore, we examined whether the same InsCtx neurons are activated during two similar inflammatory experiences. We evaluated c-Fos expression by TRAPing neurons in the initial zymosan exposure and compared them to the c-Fos-expressing neurons identified by IF, following a second zymosan exposure 14 days later (Figure S6K). Although a comparison between TRAPed neurons and neurons labeled by IF has several limitations, our findings support the concept that unique neuronal ensembles encode each immune experience, as there was only limited overlap between the neurons labeled during the two separate zymosan exposures (Figure S6L).

Stress and pain are known to play a critical role in immune regulation ((Dhabhar, 2014); Pinho-Ribeiro et al., 2017). However, we did not identify an increase in corticosterone or noradrenaline levels following our neuronal manipulation (Figures S7A and S7B). To dissect the potential effect of pain on the immune information encoded and induced by the InsCtx, we used an analgesic drug, acetaminophen, during TRAPing. To ensure that timing of the neuronal TRAPing is aligned with the maximal effect of the analgesia, we used 4-hydroxy TM (4-OHT), which has a shorter time window of activity compared to TM (DeNardo et al., 2019; Guenthner et al., 2013) (Figures S7E–S7G). In spite of the attenuated pain (Figures S7C and S7D), we found that some immune effects were still evident in this group (Figure S7H), indicating that at least part of the immune information that is encoded in the InsCtx is not mediated by pain. Yet, other effects that were abolished in the presence of analgesic suggest that pain can also alter the immune experience encoded by the brain.

Neurons in the InsCtx are anatomically connected to the colon and peritoneum

To identify the potential anatomical pathways that enable such communication between the InsCtx and these visceral sites, we used polysynaptic retrograde tracing. First, we injected a pseudorabies virus (PRV) carrying a GFP fluorescent reporter into the colons of wild-type mice (Figures 6A and 6B). After 7 days, a fluorescent signal of the PRV was seen in the InsCtx, indicating that neurons in the InsCtx can potentially deliver information to the colon (Figure 6C). However, these data do not unequivocally prove that the specific neurons included in the TRAPed ensembles can also deliver signals to the same region. Thus, we used TRAP mice and captured the neurons during colitis (Figure 6D). Then, upon recovery, we injected these mice with PRV to the colon. Indeed, we could see that some of the TRAPed neurons also expressed GFP encoded by the PRV

Figure 5. Reactivation of neuronal ensembles captured during peritonitis induces immune activation reminiscent of zymosan-induced peritonitis (ZIP)

(A) Scheme of TRAPing InsCtx neurons via different timings of TM injections, relative to ZIP, and their reactivation upon recovery. The sham viral-vector control group expressed only the fluorescent reporter.

(B) Representative composite imaging showing the expression of the injected Cre-dependent DREADD (mCherry, in red) in the InsCtx in both Gq-expressing groups (n = 4, 6 mice). Scale bar: 250 μm.

(C) Quantification of DREADD-expressing neurons in the InsCtx of both Gq groups. Student's t-test. Top right: legends indicating the trend and significance levels in the comparison between the original Zymosan administered (ZI-peritonitis) mice and their non-inflamed controls (PBS) compared to the reactivation experiment including both Gq groups, labeled before (Gq before) and during (Gq during) peritonitis, and their sham viral vector controls (Sham). Provided on the left to (D–O).

(D–M) Graphs derived from flow cytometry analysis, showing percentages of (D) monocytes, (E) granulocytes, (F) B lymphocytes, (G) TLR4$^+$ leukocytes, (H) IFNγ^+ leukocytes, (I) percentages of TLR2$^+$ cells, (J) TLR2 expression on leukocytes, (K) percentages of TLR2$^+$ DCs, and (L) TLR2 expression on DC and (M) monocytes. (N and O) (N) Percentages of activated CD4 T cells and (O) their CD69 expression (MFI). Student's t-test, one-way ANOVA and Tukey's multiple comparisons test. Two (J) and four (M) samples were excluded from the data; ROUT method for outlier detection (Q = 1%). In all bar graphs, data from individual mice are shown, and values are represented as mean ± SEM. InsCtx, insular cortex; TM, Tamoxifen; CNO, clozapine-*N*-oxide; PLF, Peritoneal lavage fluid; mLN, mesenteric lymph nodes; MFI, median fluorescence intensity; DCs, dendritic cells. Data represent at least two independent repeats. See also Figures S5, S6, and S7.

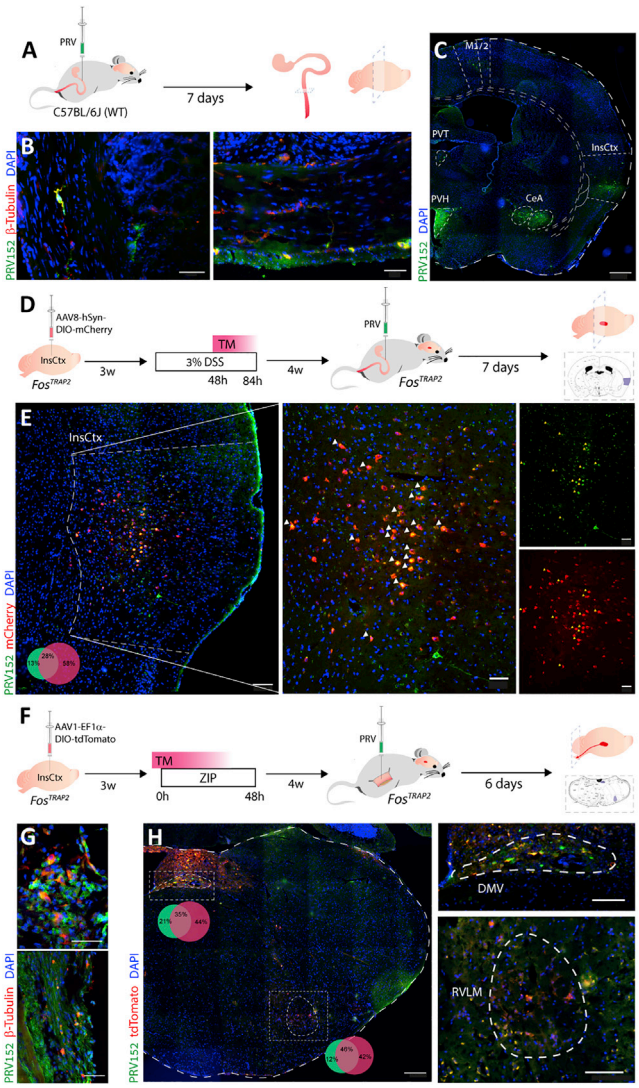

Figure 6. Transsynaptic neuronal tracing of pathways descending from the InsCtx to the colon and peritoneum

(A) PRV-152 was injected to the proximal colonic wall in C57BL/6J WT mice. Seven days later, colons and brains were harvested of for further IF analysis.

(B) Representative micrographs of the colon wall demonstrating neurons (β-tubulin$^+$, red) expressing PRV (green). Scale bar: 50 μm.

(C) Representative composite micrograph of the brain demonstrating PRV$^+$ neurons in the paraventricular nucleus of the thalamus (PVT), paraventricular nucleus of the hypothalamus (PVH), central amygdala (CeA), motor cortex (M1/2), and insular cortex (InsCtx) 7 days following PRV injection to the colon. Scale bar: 500 μm.

(D) PRV-152 injection to the proximal colonic wall in *Fos*^{TRAP2} mice that were previously treated with TM during DSS-induced colitis. Seven days later colons and brains were harvested for further IF analysis.

(E) Representative composite micrograph of the brain demonstrating PRV$^+$ neurons in the AAV-injection site of the InsCtx (neurons TRAPed during DSS-induced colitis are in red; mCherry). Arrows indicate double positive cells for PRV and mCherry. Scale bars: 100 μm (left), 50 μm (right). The Venn-diagram shows percentages of mCherry$^+$ (red), PRV$^+$ (green) and co-localized cells out of total stained cells.

(F) PRV-152 injection to the peritoneal wall in *Fos*^{TRAP2} mice that were previously treated with TM during ZIP. Six days later, peritoneal wall and brains were harvested for further IF analysis.

(G) Representative micrographs of the peritoneal wall demonstrating neurons (β-tubulin$^+$, red) expressing PRV (green). Scale bar: 50 μm.

(H) Representative composite micrographs of the brainstem demonstrating PRV$^+$ (green) and tdTomato$^+$ (AAV1, red) neurons in the dorsal motor nucleus of the vagus (DMV) and rostral ventrolateral medulla (RVLM). Scale bars: 200 μm (left), 50 μm (right). The Venn-diagrams show percentages of AAV$^+$ (red), PRV$^+$ (green) and co-localized cells out of total stained cells. TM, Tamoxifen; ZIP, Zymosan-induced peritonitis. Data represent two independent repeats.

(Figure 6E), demonstrating that neurons included in the TRAPed ensembles, which can induce local inflammation, have a direct path of communication with the colon.

In the peritonitis model, we injected the PRV in the peritoneum, but to the InsCtx, we injected a virus that has both retrograde and anterograde monosynaptic transport (AAV1) for capturing the active neurons (Figures 6F and 6G). This allowed us to identify that the PRV and AAV1 overlapped in the dorsal motor nucleus of the vagus (DMV), the vagal control center, and the rostral ventrolateral medulla (RVLM) (Figure 6H), which coordinates the sympathetic nervous system. These findings suggest that neurons TRAPed during peripheral inflammation can directly deliver messages to the peripheral sites and that these effects are mediated via the autonomic nervous system.

Inhibition of the InsCtx attenuates the cellular immune response in the colon

Since InsCtx activity can initiate and induce a peripheral immune response, it could potentially trigger or exacerbate inflammatory conditions. Indeed, changes in InsCtx activity are evident in inflammatory diseases, especially common in gut-related disorders (Chen et al., 2011; Turkiewicz et al., 2021). Therefore, we tested the possibility that inhibition of InsCtx activity may attenuate colon inflammation. We expressed in the InsCtx an inhibitory DREADD, Gi, in a Cre-independent manner and treated the mice with DSS in their drinking water while injecting them daily with CNO (Figure 7A). The reduction in InsCtx activity (Figure 7B) had a significant effect, attenuating clinical symptoms such as colon length (Figures 7C and 7D) and spleen weight (Figure 7E), but not all clinical and histological parameters were affected (Figures 7F–7H, S8A, and S8B). DREADD-induced inhibition also had a significant effect on the immune response in the colon (Figures 7I–7O and S8C–S8E), specifically, reducing the number of mucosal leukocytes (Figures 7I and 7M) and the percentage of TNF-α^+ leukocytes (Figure 7J), activated γδ (Figure 7K) and CD4 T cells (Figures 7L and 7N), and IL-6$^+$ CD4 T cells (Figure 7O). Thus, we found that many, but not all, clinical and immune parameters were attenuated by the nonspecific InsCtx inhibition. This finding suggests that targeted manipulation of the InsCtx may be a therapeutic strategy to control colon inflammation.

DISCUSSION

Our data demonstrate that neurons in the InsCtx can acquire and retrieve specific immune-related information. In the field of neuroscience, this type of information encoding is reminiscent of memory traces (Josselyn and Tonegawa, 2020; (Dudai,

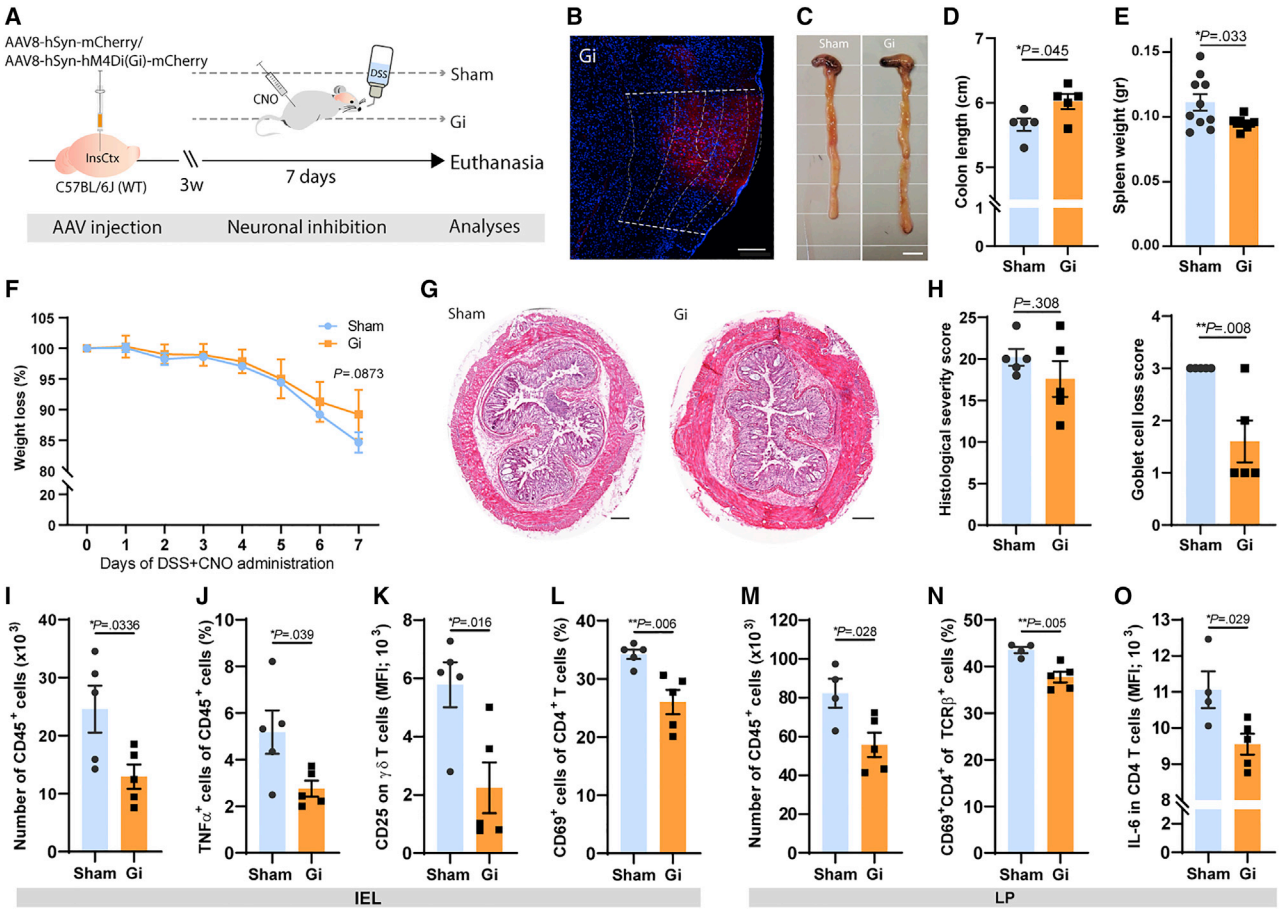

Figure 7. Inhibition of the InsCtx exerts a reduced inflammatory state during DSS-induced colitis

(A) Scheme of Cre independently expressing the inhibitory form of DREADD (Gi) or a sham virus in InsCtx neurons of C57BL/6 WT mice. Three weeks later, all mice received 3% DSS in their drinking water and daily CNO injections for 7 days.

(B) Representative micrograph showing the expression of the injected DREADD (mCherry, in red) in the InsCtx. Scale bar: 250 μm.

(C) Representative gross images of colons extracted from the Gi (right) and Sham control (left) mice. Scale bar: 1 cm.

(D–F) Measurements of colon length (D) spleen weight (E) and weight loss (F) in the Gi-expressing mice compared to their Sham controls. (D–E) Student's *t*-test, (F) Benjamini, Krieger, and Yekutieli Multiple comparisons.

(G) Representative light microscopy images of colon sections stained with H&E from the two experimental groups. Scale bar: 200 μm.

(H) Histological severity scores (left) and goblet cell loss score (right) as measured in colons stained with H&E, from both experimental groups.

(I–O) Graphs derived from flow cytometry analysis showing (I–L) IEL analysis of number of (I) leukocytes, (J) percentages of TNFα$^+$ leukocytes, (K) CD25 expression (MFI) on γδ T cells, and (L) percentages of CD69$^+$ CD4 T cells; (M–O) immune cells in the LP, (M) number of leukocytes, (N) percentages of CD69$^+$ CD4 T cells, and (O) IL-6 expression (MFI) in CD4 T cells of Gi mice compared to their Sham controls. (H–O) Student's *t*-test.

In all bar graphs, data from individual mice are shown, and values are represented as mean ± SEM. InsCtx, Insular cortex; DSS, dextran sulfate sodium; CNO, clozapine-*N*-oxide; IEL, intraepithelial lymphocytes; LP, lamina propria; MFI, median fluorescence intensity. Data represent two independent repeats. See also Figure S8.

2012)). In recent years, such memory traces were demonstrated mostly by retrieval of fear-related behavior with the reactivation of hippocampal neuronal ensembles captured during fear conditioning (Lacagnina et al., 2019; Liu et al., 2012; Ryan et al., 2015). Similarly, in our paradigm, reactivation of neurons captured under a unique inflammatory condition was sufficient to induce a related inflammatory response.

Numerous recent studies aim to understand the mechanisms that enable the brain to communicate directly with immune cells in the periphery (Dantzer, 2018; Huh and Veiga-Fernandes, 2020; Kipnis, 2016). Here, we focused on the potential mechanisms whereby the neuronal ensembles in the InsCtx can regulate local peripheral reactions, and we show that at least anatomically, these effects can be mediated via both arms of the autonomic nervous system. Subsequently, it will be interesting to identify the nature of the mechanisms that generate the diversity of the information delivered to the periphery, how it varies with context (e.g., analgesia), and how the peripheral anatomy is encoded by the autonomic nervous system. It will also be important to understand which peripheral cells receive the messages from the brain and whether they are received directly by immune cells or, alternatively, by the tissue's parenchymal cells (e.g., colon

epithelium), which may also contribute to the anatomical specificity of the induced immune responses.

A fundamental question is the nature of the evolutionary advantage for the organism in encoding such detailed and specific immune information. One possibility is that the brain, which constantly records external cues (e.g., place and odor), also records its own response to these experiences as a means to enable a more effective, anticipatory immune reaction to recurring stimuli. Nevertheless, such a potentially beneficial physiological response could also lead to maladaptive conditions. For example, it was shown almost 150 years ago that presenting patients allergic to pollen with an artificial flower is sufficient to induce an allergic response (Mackeszie, 1886). Moreover, many gut-related disorders are suggested to be psychosomatic in etiology, induced by emotionally salient experiences. The limited understanding of the underlying mechanisms of such disorders (Dinan and Cryan, 2017; Enck et al., 2016; Moloney et al., 2015) hampers the effectiveness of clinical interventions that are currently available. Our findings reveal the potential of inhibiting InsCtx activity as a means of suppressing peripheral inflammation. Thus, this study adds another perspective to the understanding of these pathological conditions and, presumably, an avenue for therapeutic intervention.

LIMITATIONS OF THE STUDY

This study introduces an experimental platform to study encoding of immune and physiological information in the brain. However, it is possible that the information that was encoded by the neuronal ensembles reflects sensory input from the tissue (gut or peritoneum) rather than a memory trace of the immune response. Such a phenomenon is distinct from the classical concept of memory.

Moreover, we focused on the InsCtx, but this brain region is most likely only a part of the neuronal representation of the immune-related information in the brain, and it does not exclude the possibility that other brain areas may be even more crucial for this process.

STAR★METHODS

Detailed methods are provided in the online version of this paper and include the following:

- KEY RESOURCES TABLE
- RESOURCE AVAILABILITY
  - Lead contact
  - Materials availability
  - Data and code availability
- EXPERIMENTAL MODEL AND SUBJECT DETAILS
  - Mice
- METHOD DETAILS
  - Stereotactic injections
  - DSS-induced colitis
  - Zymosan-induced peritonitis
  - Activity-dependent cell labeling
  - Chemogenetic neuronal manipulation
  - Tissue preparation and immunofluorescence
  - Retrograde PRV tracing
  - Histopathological scoring of colon sections
  - Clinical scoring of colitis severity
  - smFISH
  - iDISCO sample processing
  - Light-sheet imaging
  - Flow cytometry
  - Measurement of cytokine levels
  - Corticosterone and Noradrenaline measurement
  - Von Frey test
  - Illustrations
- QUANTIFICATION AND STATISTICAL ANALYSIS
  - Quantification
  - Cleared brain analysis
  - Statistical analysis

SUPPLEMENTAL INFORMATION

Supplemental information can be found online at https://doi.org/10.1016/j.cell.2021.10.013.

ACKNOWLEDGMENTS

We would like to thank J. Gross, D. Khatib, D. Derdikman, Y. Berger, and O. Barak for helpful discussions and technical support; S. Schwarzbaum for editing the manuscript and her insightful comments; A. Grau, A. Shemesh, O. Shenker, E. Suss-Toby, S. Huleihel, N. Dahan, and Y. Sakoury for technical support; and M. Schlesinger, T. Hass, R. Shofti, and the preclinical research facility team for their help with the rodent work.

This work was supported by the ERC STG, NIEMO (758952) and the Prince Center for Neurodegenerative Disorders of the Brain. A.R. is a Howard Hughes Medical Institute (HHMI)-Wellcome Trust international scholar.

AUTHOR CONTRIBUTIONS

T.K. designed and carried out all the experiments, interpreted the results, and wrote the manuscript. R.Y., M.A., M.K., N.B., H.D., and E.A. contributed to the experimental design, execution, and data analysis. T.L.B.-S. contributed to the development of the experimental design. I.Z., H. Hajjo, M.S., B.K., H. Haykin, and D.F. contributed to the execution of the experiments. O.K. contributed to the anatomical tracing. F.H. and K.R. contributed to the experimental design and the interpretation of the results. A.R. contributed to the experimental design and data interpretation and wrote the manuscript. All authors commented on the final manuscript.

DECLARATION OF INTERESTS

A.R., T.K., T.L.B.-S., and H.A.-D. have a patent application related to this work.

Received: December 19, 2020
Revised: September 5, 2021
Accepted: October 12, 2021
Published: November 8, 2021; Corrected online: November 17, 2021

REFERENCES

Ader, R., and Cohen, N. (1975). Behaviorally conditioned immunosuppression. Psychosom. Med. *37*, 333–340.

Annacker, O., Coombes, J.L., Malmstrom, V., Uhlig, H.H., Bourne, T., Johansson-Lindbom, B., Agace, W.W., Parker, C.M., and Powrie, F. (2005). Essential role for CD103 in the T cell-mediated regulation of experimental colitis. J. Exp. Med. *202*, 1051–1061.

Bábíčková, J., Tóthová, Ľ., Lengyelová, E., Bartoňová, A., Hodosy, J., Gardlík, R., and Celec, P. (2015). Sex Differences in Experimentally Induced Colitis in Mice: a Role for Estrogens. Inflammation *38*, 1996–2006.

Belevych, N., Buchanan, K., Chen, Q., Bailey, M., and Quan, N. (2010). Location-specific activation of the paraventricular nucleus of the hypothalamus by localized inflammation. Brain Behav. Immun. *24*, 1137–1147.

Ben-Shaanan, T.L., Azulay-Debby, H., Dubovik, T., Starosvetsky, E., Korin, B., Schiller, M., Green, N.L., Admon, Y., Hakim, F., Shen-Orr, S.S., and Rolls, A. (2016). Activation of the reward system boosts innate and adaptive immunity. Nat. Med. *22*, 940–944.

Ben-Shaanan, T.L., Schiller, M., Azulay-Debby, H., Korin, B., Boshnak, N., Koren, T., Krot, M., Shakya, J., Rahat, M.A., Hakim, F., and Rolls, A. (2018). Modulation of anti-tumor immunity by the brain's reward system. Nat. Commun. *9*, 2723.

Buller, K.M., and Day, T.A. (2002). Systemic administration of interleukin-1β activates select populations of central amygdala afferents. J. Comp. Neurol. *452*, 288–296.

Cash, J.L., White, G.E., and Greaves, D.R. (2009). Chapter 17. Zymosan-induced peritonitis as a simple experimental system for the study of inflammation. Methods Enzymol. *461*, 379–396.

Chassaing, B., Aitken, J.D., Malleshappa, M., and Vijay-Kumar, M. (2014). Dextran Sulfate Sodium (DSS)-Induced Colitis in Mice. Curr. Protoc. Immunol. *104*, 15.25.1–15.25.14.

Chen, J.Y.W., Blankstein, U., Diamant, N.E., and Davis, K.D. (2011). White matter abnormalities in irritable bowel syndrome and relation to individual factors. Brain Res. *1392*, 121–131.

Chovatiya, R., and Medzhitov, R. (2014). Stress, inflammation, and defense of homeostasis. Mol. Cell *54*, 281–288.

Cohen, N., Moynihan, J.A., and Ader, R. (1994). Pavlovian conditioning of the immune system. Int. Arch. Allergy Immunol. *105*, 101–106.

Craig, A.D. (2002). How do you feel? Interoception: the sense of the physiological condition of the body. Nat. Rev. Neurosci. *3*, 655–666.

Craig, A.D. (2003). Interoception: the sense of the physiological condition of the body. Curr. Opin. Neurobiol. *13*, 500–505.

Critchley, H.D., and Harrison, N.A. (2013). Visceral influences on brain and behavior. Neuron *77*, 624–638.

Dantzer, R. (2018). Neuroimmune interactions: From the brain to the immune system and vice versa. Physiol. Rev. *98*, 477–504.

DeNardo, L.A., Liu, C.D., Allen, W.E., Adams, E.L., Friedmann, D., Fu, L., Guenthner, C.J., Tessier-Lavigne, M., and Luo, L. (2019). Temporal evolution of cortical ensembles promoting remote memory retrieval. Nat. Neurosci. *22*, 460–469.

Dhabhar, F.S. (2014). Effects of stress on immune function: the good, the bad, and the beautiful. Immunol. Res. *58*, 193–210.

Dinan, T.G., and Cryan, J.F. (2017). The Microbiome-Gut-Brain Axis in Health and Disease. Gastroenterol. Clin. North Am. *46*, 77–89.

Doenlen, R., Krügel, U., Wirth, T., Riether, C., Engler, A., Prager, G., Engler, H., Schedlowski, M., and Pacheco-López, G. (2011). Electrical activity in rat cortico-limbic structures after single or repeated administration of lipopolysaccharide or staphylococcal enterotoxin B. Proc. Biol. Sci. *278*, 1864–1872.

Dudai, Y. (2012). The restless engram: consolidations never end. Annu. Rev. Neurosci. *35*, 227–247.

Enck, P., Aziz, Q., Barbara, G., Farmer, A.D., Fukudo, S., Mayer, E.A., Niesler, B., Quigley, E.M.M., Rajilić-Stojanović, M., Schemann, M., et al. (2016). Irritable bowel syndrome. Nat. Rev. Dis. Primers *2*, 16014.

Fung, T.C., Olson, C.A., and Hsiao, E.Y. (2017). Interactions between the microbiota, immune and nervous systems in health and disease. Nat. Neurosci. *20*, 145–155.

Garber, J.C., Barbee, R.W., Bielitzki, J.T., Clayton, L.A., Donovan, J.C., Hendriksen, C.F.M., Kohn, D.F., Lipman, N.S., Locke, P.A., Melcher, J., et al. (2011). Guide for The Care and Use of Laboratory Animals (The National Academies Press).

Gassen, S., Van, Callebaut, B., Van Helden, M.J., Lambrecht, B.N., Demeester, P., Dhaene, T., and Saeys, Y. (2015). FlowSOM: Using Self-Organizing Maps for Visualization and Interpretation of Cytometry Data. Cytometry A *87*, 636–645.

Goehler, L.E., Gaykema, R.P.A., Hansen, M.K., Anderson, K., Maier, S.F., and Watkins, L.R. (2000). Vagal immune-to-brain communication: a visceral chemosensory pathway. Auton. Neurosci. *85*, 49–59.

Gogolla, N. (2017). The insular cortex. Curr. Biol. *27*, R580–R586.

Guenthner, C.J., Miyamichi, K., Yang, H.H., Heller, H.C., and Luo, L. (2013). Permanent genetic access to transiently active neurons via TRAP: targeted recombination in active populations. Neuron *78*, 773–784.

Hadamitzky, M., Lückemann, L., Pacheco-López, G., and Schedlowski, M. (2020). Pavlovian conditioning of immunological and neuroendocrine functions. Physiol. Rev. *100*, 357–405.

Han, W., Tellez, L.A., Perkins, M.H., Shammah-Lagnado, S.J., De Lartigue, G., and De Araujo Correspondence, I.E. (2018). A Neural Circuit for Gut-Induced Reward In Brief. Cell *175*, 1–14.

Hanken, K., Eling, P., and Hildebrandt, H. (2014). The representation of inflammatory signals in the brain - a model for subjective fatigue in multiple sclerosis. Front. Neurol. *5*, 264.

Harrison, N.A., Brydon, L., Walker, C., Gray, M.A., Steptoe, A., Dolan, R.J., and Critchley, H.D. (2009). Neural origins of human sickness in interoceptive responses to inflammation. Biol. Psychiatry *66*, 415–422.

Hobday, D.I., Aziz, Q., Thacker, N., Hollander, I., Jackson, A., and Thompson, D.G. (2001). A study of the cortical processing of ano-rectal sensation using functional MRI. Brain *124*, 361–368.

Hoytema van Konijnenburg, D.P., Reis, B.S., Pedicord, V.A., Farache, J., Victora, G.D., and Mucida, D. (2017). Intestinal Epithelial and Intraepithelial T Cell Crosstalk Mediates a Dynamic Response to Infection. Cell *171*, 783–794.e13.

Huh, J.R., and Veiga-Fernandes, H. (2020). Neuroimmune circuits in inter-organ communication. Nat. Rev. Immunol. *20*, 217–228.

Hyman, J.M., Ma, L., Balaguer-Ballester, E., Durstewitz, D., and Seamans, J.K. (2012). Contextual encoding by ensembles of medial prefrontal cortex neurons. Proc. Natl. Acad. Sci. USA *109*, 5086–5091.

Jain, P., Materazzi, S., De Logu, F., Rossi Degl'Innocenti, D., Fusi, C., Li Puma, S., Marone, I.M., Coppi, E., Holzer, P., Geppetti, P., and Nassini, R. (2020). Transient receptor potential ankyrin 1 contributes to somatic pain hypersensitivity in experimental colitis. Sci. Rep. *10*, 8632.

Josselyn, S.A., and Tonegawa, S. (2020). Memory engrams: Recalling the past and imagining the future. Science *367*, eaaw4325.

Jóźwiak-Bebenista, M., and Nowak, J.Z. (2014). Paracetamol: mechanism of action, applications and safety concern. Acta Pol. Pharm. *71*, 11–23.

Kaelberer, M.M., Buchanan, K.L., Klein, M.E., Barth, B.B., Montoya, M.M., Shen, X., and Bohórquez, D.V. (2018). A gut-brain neural circuit for nutrient sensory transduction. Science *361*, eaat5236.

Kipnis, J. (2016). Multifaceted interactions between adaptive immunity and the central nervous system. Science *353*, 766–771.

Kipnis, J. (2018). Immune system: The "seventh sense". J. Exp. Med. *215*, 397–398.

Koelink, P.J., Wildenberg, M.E., Stitt, L.W., Feagan, B.G., Koldijk, M., van 't Wout, A.B., Atreya, R., Vieth, M., Brandse, J.F., Duijst, S., et al. (2018). Development of Reliable, Valid and Responsive Scoring Systems for Endoscopy and Histology in Animal Models for Inflammatory Bowel Disease. J. Crohn's Colitis *12*, 794–803.

Lacagnina, A.F., Brockway, E.T., Crovetti, C.R., Shue, F., McCarty, M.J., Sattler, K.P., Lim, S.C., Santos, S.L., Denny, C.A., and Drew, M.R. (2019). Distinct hippocampal engrams control extinction and relapse of fear memory. Nat. Neurosci. *22*, 753–761.

Liang, J., Huang, H.I., Benzatti, F.P., Karlsson, A.B., Zhang, J.J., Youssef, N., Ma, A., Hale, L.P., and Hammer, G.E. (2016). Inflammatory Th1 and Th17 in the Intestine Are Each Driven by Functionally Specialized Dendritic Cells with Distinct Requirements for MyD88. Cell Rep. *17*, 1330–1343.

Liu, X., Ramirez, S., Pang, P.T., Puryear, C.B., Govindarajan, A., Deisseroth, K., and Tonegawa, S. (2012). Optogenetic stimulation of a hippocampal engram activates fear memory recall. Nature *484*, 381–385.

Mackeszie, J.N. (1886). THE PRODUCTION OF THE SO-CALLED "ROSE COLD" BY MEANS OF AN ARTIFICIAL ROSE. Am. J. Med. Sci. *181*, 45–56.

Madisen, L., Zwingman, T.A., Sunkin, S.M., Oh, S.W., Zariwala, H.A., Gu, H., Ng, L.L., Palmiter, R.D., Hawrylycz, M.J., Jones, A.R., et al. (2010). A robust and high-throughput Cre reporting and characterization system for the whole mouse brain. Nat. Neurosci. *13*, 133–140.

Mankin, E.A., Sparks, F.T., Slayyeh, B., Sutherland, R.J., Leutgeb, S., and Leutgeb, J.K. (2012). Neuronal code for extended time in the hippocampus. Proc. Natl. Acad. Sci. USA *109*, 19462–19467.

Mayer, E.A. (2011). Gut feelings: the emerging biology of gut-brain communication. Nat. Rev. Neurosci. *12*, 453–466.

McDonald, B., Pittman, K., Menezes, G.B., Hirota, S.A., Slaba, I., Waterhouse, C.C.M., Beck, P.L., Muruve, D.A., and Kubes, P. (2010). Intravascular Danger Signals Guide Neutrophils to Sites of Sterile Inflammation. Science *330*, 362–366.

Moloney, R.D., O'Mahony, S.M., Dinan, T.G., and Cryan, J.F. (2015). Stress-induced visceral pain: toward animal models of irritable-bowel syndrome and associated comorbidities. Front. Psychiatry *6*, 15.

Montalbano, M.J., and Shane Tubbs, R. (2018). Lateralization of the Insular Cortex. Island of Reil (Insula) in the Human Brain (Cham: Springer International Publishing), pp. 129–132.

Motulsky, H.J., and Brown, R.E. (2006). Detecting outliers when fitting data with nonlinear regression - a new method based on robust nonlinear regression and the false discovery rate. BMC Bioinformatics *7*, 123.

Muller, P.A., Schneeberger, M., Matheis, F., Wang, P., Kerner, Z., Ilanges, A., Pellegrino, K., del Mármol, J., Castro, T.B.R., Furuichi, M., et al. (2020). Microbiota modulate sympathetic neurons via a gut–brain circuit. Nature *583*, 441–446.

Pacheco-López, G., Niemi, M.B., Kou, W., Härting, M., Fandrey, J., and Schedlowski, M. (2005). Neural substrates for behaviorally conditioned immunosuppression in the rat. J. Neurosci. *25*, 2330–2337.

Park, Y.H., Kim, N., Shim, Y.K., Choi, Y.J., Nam, R.H., Choi, Y.J., Ham, M.H., Suh, J.H., Lee, S.M., Lee, C.M., et al. (2015). Adequate Dextran Sodium Sulfate-induced Colitis Model in Mice and Effective Outcome Measurement Method. J. Cancer Prev. *20*, 260–267.

Pavlov, V.A., and Tracey, K.J. (2017). Neural regulation of immunity: molecular mechanisms and clinical translation. Nat. Neurosci. *20*, 156–166.

Pinho-Ribeiro, F.A., Verri, W.A., Jr., and Chiu, I.M. (2017). Nociceptor Sensory Neuron-Immune Interactions in Pain and Inflammation. Trends Immunol. *38*, 5–19.

Powell, N., Walker, M.M., and Talley, N.J. (2017). The mucosal immune system: master regulator of bidirectional gut-brain communications. Nat. Rev. Gastroenterol. Hepatol. *14*, 143–159.

Prass, K., Meisel, C., Höflich, C., Braun, J., Halle, E., Wolf, T., Ruscher, K., Victorov, I.V., Priller, J., Dirnagl, U., et al. (2003). Stroke-induced immunodeficiency promotes spontaneous bacterial infections and is mediated by sympathetic activation reversal by poststroke T helper cell type 1-like immunostimulation. J. Exp. Med. *198*, 725–736.

Ramírez-Amaya, V., and Bermúdez-Rattoni, F. (1999). Conditioned enhancement of antibody production is disrupted by insular cortex and amygdala but not hippocampal lesions. Brain Behav. Immun. *13*, 46–60.

Ramírez-Amaya, V., Alvarez-Borda, B., Ormsby, C.E., Martínez, R.D., Pérez-Montfort, R., and Bermúdez-Rattoni, F. (1996). Insular cortex lesions impair the acquisition of conditioned immunosuppression. Brain Behav. Immun. *10*, 103–114.

Ramírez-Amaya, V., Alvarez-Borda, B., and Bermúdez-Rattoni, F. (1998). Differential effects of NMDA-induced lesions into the insular cortex and amygdala on the acquisition and evocation of conditioned immunosuppression. Brain Behav. Immun. *12*, 149–160.

Reardon, C., Murray, K., and Lomax, A.E. (2018). Neuroimmune Communication in Health and Disease. Physiol. Rev. *98*, 2287–2316.

Renier, N., Wu, Z., Simon, D.J., Yang, J., Ariel, P., and Tessier-Lavigne, M. (2014). iDISCO: a simple, rapid method to immunolabel large tissue samples for volume imaging. Cell *159*, 896–910.

Renier, N., Adams, E.L., Kirst, C., Wu, Z., Azevedo, R., Kohl, J., Autry, A.E., Kadiri, L., Umadevi Venkataraju, K., Zhou, Y., et al. (2016). Mapping of Brain Activity by Automated Volume Analysis of Immediate Early Genes. Cell *165*, 1789–1802.

Rogan, S.C., and Roth, B.L. (2011). Remote control of neuronal signaling. Pharmacol. Rev. *63*, 291–315.

Ryan, T.J., Roy, D.S., Pignatelli, M., Arons, A., and Tonegawa, S. (2015). Engram cells retain memory under retrograde amnesia. Science *348*, 1007–1013.

Schindelin, J., Arganda-Carreras, I., Frise, E., Kaynig, V., Longair, M., Pietzsch, T., Preibisch, S., Rueden, C., Saalfeld, S., Schmid, B., et al. (2012). Fiji: an open-source platform for biological-image analysis. Nat. Methods *9*, 676–682.

Sergeeva, M., Rech, J., Schett, G., and Hess, A. (2015). Response to peripheral immune stimulation within the brain: magnetic resonance imaging perspective of treatment success. Arthritis Res. Ther. *17*, 268.

Silberman, D.M., Wald, M.R., and Genaro, A.M. (2003). Acute and chronic stress exert opposing effects on antibody responses associated with changes in stress hormone regulation of T-lymphocyte reactivity. J. Neuroimmunol. *144*, 53–60.

Sweis, B.M., Mau, W., Rabinowitz, S., and Cai, D.J. (2021). Dynamic and heterogeneous neural ensembles contribute to a memory engram. Curr. Opin. Neurobiol. *67*, 199–206.

Thayer, J.F., and Sternberg, E.M. (2009). Neural concomitants of immunity—Focus on the vagus nerve. Neuroimage *47*, 908–910.

Turkiewicz, J., Bhatt, R.R., Wang, H., Vora, P., Krause, B., Sauk, J.S., Jacobs, J.P., Bernstein, C.N., Kornelsen, J., Labus, J.S., et al. (2021). Altered brain structural connectivity in patients with longstanding gut inflammation is correlated with psychological symptoms and disease duration. Neuroimage Clin. *30*, 102613.

Veiga-Fernandes, H., and Mucida, D. (2016). Neuro-Immune Interactions at Barrier Surfaces. Cell *165*, 801–811.

Willemze, R.A., Luyer, M.D., Buurman, W.A., and de Jonge, W.J. (2015). Neural reflex pathways in intestinal inflammation: hypotheses to viable therapy. Nat. Rev. Gastroenterol. Hepatol. *12*, 353–362.

Wong, C.H.Y., Jenne, C.N., Lee, W.-Y., Léger, C., and Kubes, P. (2011). Functional innervation of hepatic iNKT cells is immunosuppressive following stroke. Science *334*, 101–105.

Yan, Y., Kolachala, V., Dalmasso, G., Nguyen, H., Laroui, H., Sitaraman, S.V., and Merlin, D. (2009). Temporal and spatial analysis of clinical and molecular parameters in dextran sodium sulfate induced colitis. PLoS ONE *4*, e6073.

Zhang, Y.H., Lu, J., Elmquist, J.K., and Saper, C.B. (2000). Lipopolysaccharide activates specific populations of hypothalamic and brainstem neurons that project to the spinal cord. J. Neurosci. *20*, 6578–6586.

Ziv, Y., Burns, L.D., Cocker, E.D., Hamel, E.O., Ghosh, K.K., Kitch, L.J., El Gamal, A., and Schnitzer, M.J. (2013). Long-term dynamics of CA1 hippocampal place codes. Nat. Neurosci. *16*, 264–266.

STAR★METHODS

KEY RESOURCES TABLE

REAGENT or RESOURCE	SOURCE	IDENTIFIER
Antibodies		
Mouse anti-NeuN	Sigma-Aldrich	Cat# MAB377; RRID: AB_2298772
Rabbit anti-GFAP	Agilent	Cat# ZO334
Chicken anti-GFAP	Abcam	Cat# ab4674; RRID: AB_304558
Chicken anti-mCherry	Abcam	Cat# ab205402; RRID: AB_2722769
Alexa-flour 700-conjugated anti-CD45	BioLegend	Cat# 103128; RRID: AB_493715
Rabbit anti-c-Fos	Abcam	Cat# ab190289; RRID: AB_2737414
Alexa Fluor 488-conjugated anti-mouse IgG	Jackson ImmunoResearch laboratories	Cat# 715-545-151; RRID: AB_2341099
Cy5-conjugated anti-rabbit IgG	Jackson ImmunoResearch laboratories	Cat# 111-175-144; RRID: AB_2338013
Cy5-conjugated anti-rat IgG	Jackson ImmunoResearch laboratories	Cat# 112-175-167; RRID: AB_2338264
Alexa Fluor 568-conjugated anti-chicken IgY	Invitrogen	Cat# A1104; RRID: AB_141874
Alexa Fluor 488-conjugated anti-chicken IgG	Jackson ImmunoResearch laboratories	Cat# 703-545-155; RRID: AB_2340375
Alexa Fluor 568-conjugated anti-rat IgG	Invitrogen	Cat# A11077; RRID: AB_141874
Chicken anti-GFP	Abcam	Cat# ab13970; RRID: AB_300798
Rabbit anti-β3 tubulin	Abcam	Cat# ab18207; RRID: AB_444319
Alexa Fluor 568-conjugated anti-rabbit IgG	Invitrogen	Cat# A11011; RRID: AB_143157
Rabbit anti-ZO1 IgG	Abcam	Cat# ab221547; RRID: AB_2892660
Biotin-conjugated rat anti Ep-CAM	BioLegend	Cat# 118204; RRID: AB_1134178
Rabbit anti-lysozyme	Abcam	Cat# ab108508; RRID: AB_10861277
Alexa Fluor 647-conjugated anti-TLR2	BioLegend	Cat# 121809; RRID: AB_604146
Biotin-conjugated anti-TLR4	BioLegend	Cat# 145409; RRID: AB_2566030
Biotin-conjugated anti-IL-12/IL-23	BioLegend	Cat# 505302; RRID: AB_315374
Brilliant violet 605-conjugated streptavidin	BioLegend	Cat# 405229
Biotin-conjugated anti-CD69	BioLegend	Cat# 104504; RRID: AB_313107
Alexa Fluor 488-conjugated streptavidin	Jackson ImmunoResearch laboratories	Cat# 016-540-084; RRID: AB_2337249
Brilliant violet 650-conjugated anti-CD69	BioLegend	Cat# 104541; RRID: AB_2616934
PE/Cy7-conjugated anti-IFN-γ	BioLegend	Cat# 505826; RRID: AB_2295770
PerCP/Cy5.5-conjugated anti-CD11b	BioLegend	Cat# 101228; RRID: AB_893232
APC-conjugated anti-F4/80	BioLegend	Cat# 123116; RRID: AB_893481
APC/Cy7-conjugated anti-F4/80	BioLegend	Cat# 123118; RRID: AB_893477
FITC-conjugated anti-Ly6G	BioLegend	Cat# 127606; RRID: AB_1236494
Alexa Fluor 700-conjugated anti-Ly6G	BioLegend	Cat# 127622; RRID: AB_10643269
Brilliant violet 510-conjugated anti-Gr-1	BioLegend	Cat# 108438; RRID: AB_2562215
Brilliant violet 510-conjugated anti-Ly6C	BioLegend	Cat# 128033; RRID: AB_2562351
FITC-conjugated anti-Ly6C	BioLegend	Cat# 128006; RRID: AB_1186135
PerCP-conjugated anti-CD8a	BioLegend	Cat# 100732; RRID: AB_893423
Alexa Fluor 488-conjugated anti-CD8	BioLegend	Cat# 100723; RRID: AB_389304
APC-conjugated anti-CD4	BioLegend	Cat# 100412; RRID: AB_312697
PE/Dazzle 594-conjugated anti CD4	BioLegend	Cat# 100456; RRID: AB_2565845
PE/Cy7-conjugated anti-CD11c	BioLegend	Cat# 117318; RRID: AB_493568
PE/Dazzle 594-conjugated anti-CD11c	BioLegend	Cat# 117348; RRID: AB_2563655
Alexa Fluor 488-conjugated anti-I-A/I-E	BioLegend	Cat# 107616; RRID: AB_493523
Pacific blue-conjugated anti-I-A/I-E	BioLegend	Cat# 107620; RRID: AB_493527
PE-conjugated anti-TCRγδ	BioLegend	Cat# 118108; RRID: AB_313832

(*Continued on next page*)

Continued

REAGENT or RESOURCE	SOURCE	IDENTIFIER
APC-conjugated anti-TCR γδ	BioLegend	Cat# 118116; RRID: AB_1731813
Pacific-blue-conjugated anti-TCRβ	BioLegend	Cat# 109226; RRID: AB_1027649
PE/Cy7-conjugated anti-CD25	BioLegend	Cat# 102016; RRID: AB_312865
Brilliant violet 605-conjugated anti-CD62L	BioLegend	Cat# 104438; RRID: AB_2563058
Brilliant violet 510-conjugated anti-CD44	BioLegend	Cat# 103044; RRID: AB_2650923
Brilliant-violet-605-conjugated anti-CD103	BioLegend	Cat# 121433; RRID: AB_2629724
PE/Cy7-conjugated anti-CD19	BioLegend	Cat# 115520; RRID: AB_313655
FITC-conjugated anti-TNFα	BioLegend	Cat# 506304; RRID: AB_315425
PE/Cy7-conjugated anti-IL-2	BioLegend	Cat# 503832; RRID: AB_2561750
PerCP/Cy5.5-conjugated anti-IL-22	BioLegend	Cat# 516411; RRID: AB_2563373
PE-conjugated anti-IL-6	BioLegend	Cat# 504504; RRID: AB_315338
PE-conjugated anti-IL-13	BioLegend	Cat# 159403; RRID: AB_2832569
Brilliant violet 510-conjugated anti-IL-17	BioLegend	Cat# 506933; RRID: AB_2562668
Bacterial and virus strains		
AAV8-hSyn-DIO-hM3D(Gq)-mCherry	ELSC vector core	N/A
AAV8-hSyn-DIO-mCherry	VVF Zurich	Cat# v116-8
AAV8-hSyn-hM3D(Gq)-mCherry	VVF Zurich	Cat# v89-8
AAV8-hSyn-mCherry	ELSC vector core	N/A
AAV1-EF1a-DIO-tdTomato	ELSC vector core	N/A
AAV8-hSyn-hM4Di(Gi)-mCherry	ELSC vector core	N/A
Pseudorabies virus Bartha strain 152 (PRV −152 (GFP))	Laboratory of O. Kobiler	N/A
AAV8-hSyn-EGFP	UNC vector core	N/A
Chemicals, peptides, and recombinant proteins		
Dextran Sulfate sodium (DSS)	TdB	Cat# DB001
Zymosan A	Sigma-Aldrich	Cat# Z4250
Tamoxifen	Sigma-Aldrich	Cat# T5648
4-Hydroxytamoxifen(4-OHT)	Sigma-Aldrich	Cat# H-6278
Clozapine-*N*-oxide (CNO)	Sigma-Aldrich	Cat# C-0832
Stellarris hybridization buffer	Biosearch Technologies	Cat# SMF-HB1
Stellarris wash buffer A	Biosearch Technologies	Cat# SMF-WA1
Stellarris wash buffer B	Biosearch Technologies	Cat# SMF-WB1
DAPI	Sigma-Aldrich	Cat# D9542
Dichloromethane (DCM)	Bio-Lab	Cat# 75-09-2
Dibenzyl ether (DBE)	Sigma-Aldrich	Cat# 108014
DAPI Fluoromount-G® Mounting Medium	SouthernBiotech	Cat# 0100-20
Acetaminophen	USP	Cat# 1003009
FastGreen	Sigma-Aldrich	Cat# F7252
Lysis buffer	BD biosciences	Cat# 555-899; RRID: AB_2869057
Critical commercial assays		
Lamina propria dissociation kit	Miltenyi Biotec	Cat# 130-097-410
Zombie Aqua dye solution	Biolegend	Cat# 423106
BD Cytofix/Cytoperm kit	BD Biosciences	Cat# 555028; RRID: AB_2869013
Stellaris FISH Probes, Custom Assay with Quasar® 670 Dye	Biosearch Technologies	Cat# SMF-1065-5-BS
TNF-α ELISA kit	PeproTech	Cat# 900-M54
IL-6 ELISA kit	PeproTech	Cat# 900-K50
IL-17 ELISA kit	PeproTech	Cat# 900-K392

(*Continued on next page*)

Continued

REAGENT or RESOURCE	SOURCE	IDENTIFIER
IL-10 ELISA kit	PeproTech	Cat# 900-M53
Noradrenaline ELISA kit	IBL America	Cat# IB89537
Corticosterone ELISA kit	Enzo Life Sciences	Cat# ADI-900-097; RRID: AB_2307314
Experimental models: Organisms/strains		
Mouse: FosTRAP1 (B6.129(Cg)-Fostm1.1(cre/ERT2) Luo/J)	Jackson Laboratory	Cat# 021882
Mouse: FosTRAP2 (Fostm2.1(icre/ERT2)Luo/J)	Jackson Laboratory	Cat# 030323
Mouse: Ai14D (B6;129S6-Gt(ROSA)26Sortm14(CAG-tdTomato)Hze/J)	Jackson Laboratory	Cat# 007908
Mouse: C57BL/6JOlaHsd	ENVIGO	Cat # 2BL/606
Mouse: TRAP-tdTomato (B6; Gt(ROSA) 26Sortm14(CAG-tdTomato)Hze- Fostm2.1(icre/ERT2) Luo/J)	Asya Rolls Lab	N/A
Software and algorithms		
Fiji software	Schindelin et al., 2012	https://imagej.net/software/fiji/
ZEN 2 (blue edition) software	Carl Zeiss	https://www.zeiss.com/microscopy/int/products/microscope-software/zen.html
Prism 9 software	GraphPad	https://www.graphpad.com/scientific-software/prism/
Flowjo 10.08 software	BD Biosciences	https://www.flowjo.com/solutions/flowjo/downloads
ClearMap	Renier et al., 2016	https://www.idisco.info/
Other		
Axio imager M2 microscope	Carl Zeiss	Cat# 430004-9902
gentleMACS Dissociator	Miltenyi Biotec	Cat# 130-093-235
Lightsheet 7	Carl Zeiss	https://www.zeiss.com/microscopy/int/products/imaging-systems/lattice-lightsheet-7.html
CytoFLEX S	Beckman coulter	Cat# B75442; RRID:
PANNORAMIC 250 Flash III	3DHistech	https://www.3dhistech.com/research/pannoramic-digital-slide-scanners/pannoramic-250-flash-iii/
Quintessential Stereotaxic Injector (QSI)	Stoelting	Cat# 53311
5 μl Syringe	Hamilton	Cat# 7633-01
Nanofil Syringe 10 Microliter	WPI	Cat# NANOFIL
33 g blunt NanoFil needle	WPI	Cat# NF33BL-2
0.9-2mm Stainless steel beads	NextAdvance	Cat# SSB14B
3.2mm Stainless steel beads	NextAdvance	Cat# SSB32
Bullet Blender Storm 24	NextAdvance	Cat# BBY24M
Fold-Up Monofilaments	Baseline	Cat# 12-1743

RESOURCE AVAILABILITY

Lead contact

Further information and requests for resources and reagents should be directed to and will be fulfilled by the lead contact, Asya Rolls (rolls@technion.ac.il).

Materials availability

This study did not generate new unique reagents.

Data and code availability

- Microscopy data reported in this paper will be shared by the lead contact upon request.

- This paper does not report original code.
- Any additional information required to reanalyze the data reported in this paper is available from the lead contact upon request.

EXPERIMENTAL MODEL AND SUBJECT DETAILS

Mice

All experiments were performed in accordance with the National Institutes of Health Guide for the Care and Use of Laboratory Animals (Garber et al., 2011). All procedures and protocols were approved by the Technion Administrative Panel of Laboratory Animal Care. Male or female adult (8-12 weeks of age; 20-25 g) Fos^{TRAP1} (Jackson Laboratory; B6.129(Cg)-*Fos*$^{tm1.1(cre/ERT2)Luo}$/J; stock #021882), Fos^{TRAP2} (Jackson Laboratory; *Fos*$^{tm2.1(icre/ERT2)Luo}$/J; stock #030323) transgenic mice were used for the InsCtx activity-dependent labeling experiments; Ai14D mice (Jackson Laboratory; B6;129S6-Gt(ROSA)26Sor$^{tm14(CAG-tdTomato)Hze}$/J; Stock #007908) were crossed with Fos^{TRAP2} for whole-brain activity-dependent labeling analysis; and C57BL/6J mice (Jackson Laboratory; C57BL/6J; stock #000664) were used for the characterization of the DSS-induced colitis, Zymosan-induced peritonitis, retrograde neuronal tracing and the Cre-independent InsCtx activation and inhibition experiments. Mice were maintained under specific-pathogen-free (SPF) conditions on a 12 h light: 12 h dark cycle (lights on at 07:00) and housed in groups of 2-5 mice per cage, with food and water *ad libitum*. In experiments including DSS-induced colitis, only male mice were used, due to previously documented sex-derived variability in this experimental model (Bábíčková et al., 2015). Otherwise, mice were randomly assigned to experimental groups.

METHOD DETAILS

Stereotactic injections

Viral vectors and viral vector plasmids were designed and produced by the Viral Vector Facility (VVF) of the Neuroscience Center Zurich, UNC vector core and ELSC Vector Core Facility. For virus delivery, mice were anesthetized with a ketamine-xylazine mixture (ketamine 80 mg per kg body weight (mg/kg); xylazine 15-20 mg/kg; Sigma-Aldrich) in sterile saline (0.9% NaCl). After shaving and sterilization of the head, mice were placed on a sterile surgical pad on top of a heating pad. Ophthalmic ointment (Duratears, Alcon) was placed over the eyes to prevent dehydration and the incision site was sterilized. Upon loss of recoil paw compression, a midline incision was made from above the forehead to the ears line, exposing the skull. After skull exposure, mice were fixed in the stereotactic frame (Stoelting) and carefully drilled through the skull, just above the target injection site. Using a 10 μL syringe with a blunt metal needle (Nanofil), placed in a Stoelting Quintessential Stereotaxic Injector (QSI), we validated that the skull was straight at all plains. We then slowly lowered the syringe into the injection site and left the needle in place for 5 minutes, both before and after the injection. We injected 0.40 μL of virus (either AAV8-hSyn-DIO-hM3D(Gq)-mCherry, AAV8-hSyn-DIO-mCherry, AAV8-hSyn-hM3D(Gq)-mCherry, AAV8-hSyn-mCherry, AAV8-hSyn-hM4Di(Gi)-mCherry, or AAV1-EF1a-DIO-tdTomato) at 0.07 μL per min into the right posterior InsCtx (AP, −0.35 mm; ML, 4.0 mm; DV, −3.83 mm; relative to bregma). For double virus injections, a mixture of 0.15 μL of AAV8-hSyn-EGFP and 0.25 μL of AAV8-hSyn-DIO-mCherry per injection was used. Following injection, the incision was closed using a tissue adhesive (VetBond) and sterilized with Polydine ointment. Mice showing signs of physical distress and pain were excluded from the experiment. Further procedures of the experiments were performed at least 21 days after surgery to ensure the expression of the virus and to avoid analyzing the immediate immune response that could be induced by the injection itself. Stereotactic injection sites were verified using fluorescence microscopy.

DSS-induced colitis

For the induction of colon inflammation (colitis) during neuronal labeling, mice were administered 3% DSS (dextran sulfate sodium, TdB consultancy) in their drinking water for 84 h. This duration of DSS administration was chosen after calibration experiments and previous studies (Chassaing et al., 2014; Yan et al., 2009), indicating that this time point was long enough for mice to exhibit signs of colon inflammation and yet, short enough to allow complete recovery within 4 weeks. In the InsCtx inhibition experiments (Figure 7) 3% DSS was administered for 7 consecutive days. Fresh DSS solutions were prepared every 2 days. During the administration period, mice were monitored for their general condition: body weight, stool consistency, and signs of illness including hunched posture and dehydrated eyes and skin.

Zymosan-induced peritonitis

For peritonitis induction, we used Zymosan A prepared from *Saccharomyces cerevisiae* cell wall (Sigma-Aldrich). 20 mg of Zymosan were dissolved in 1 mL of sterile HBSS (without Ca^{+2} and Mg^{+2}, Biological Industries), during heating in a boiling water bath for 20 min. We sonicated the solution for 20 min, washed twice with HBSS (1200 rpm, 10 min) and resuspended in HBSS to a concentration of 20 mg/ml. The Zymosan solution was aliquoted and kept at −80°C. Upon use, the Zymosan solution was diluted in sterile PBS to a concentration of 20 μg/ml and a volume of 0.5 mL was administered to each mouse via intraperitoneal (i.p.) injections (10 μg of Zymosan per peritoneal cavity). As previously described (Cash et al., 2009), this dose is sufficient to induce a well-characterized inflammatory response, which is confined to the peritoneal cavity, and resolves within 48 h after induction.

Activity-dependent cell labeling

Tamoxifen (TM, Sigma-Aldrich) was dissolved in corn oil (Sigma-Aldrich) to a concentration of 20 mg/ml and kept at 4°C until use (up to 12 h). To enable a Cre-dependent expression of the target gene (either Gq-DREADD or fluorescent reporter) in active neurons, 150 mg/kg of the TM solution was injected i.p., 24 h prior to the immunological event of interest. In the colitis model TM was injected either 48 h before DSS administration, 48 h into DSS treatment, or 7 d after cessation (for capturing InsCtx neurons active during a healthy state, colitis or the recovery phase, respectively). In the peritonitis model TM was injected 48 h or 2 h before Zymosan administration (for capturing InsCtx neurons active during a healthy state or peritonitis, respectively).

4-Hydroxytamoxifen (4-OHT, Sigma-Aldrich) was dissolved at 20 mg/ml in ethanol by shaking at 37°C for 15 min and was then aliquoted and stored at −20°C for up to several weeks. Before use, 4-OHT was re-dissolved in ethanol by shaking at 37°C for 15 min, corn oil (Sigma-Aldrich) was added to give a final concentration of 10 mg/ml 4-OHT, and the ethanol was evaporated by vacuum using centrifugation. A dose of 50 mg/kg of the final 4-OHT solution was injected i.p., 30 min prior to the immunological event of interest (48 h before or right before Zymosan administration, with or without Acetaminophen).

Chemogenetic neuronal manipulation

To activate or inhibit DREADD-expressing neurons in the InsCtx (Gq or Gi, respectively), all mice were i.p. injected with CNO (1 mg/kg; Sigma-Aldrich) in sterile saline, 4 weeks after TM or 4-OHT administration. In the DSS experiments, CNO was injected for 4 (Gq-experiments) or 7 (Gi-experiments) days at 24-hour intervals; in the Zymosan experiments, a single dose of CNO was administered 24 h prior to euthanizing the mice. For c-Fos evaluation, an additional CNO injection was administered 90 min before euthanasia. Of note, in all experiments, mice in all groups were injected with CNO to control for the potential effects of CNO (Rogan and Roth, 2011).

Tissue preparation and immunofluorescence

Validation of the virus injection site, evaluation of DREADDs' activity and c-Fos expression, analysis of neuronal phenotype in the brain, assessment of paneth cells and adhesion molecules, and validation of flow cytometry results in colonic tissues were performed by immunofluorescence staining and fluorescence microscopy. Mice were euthanized, and their brains or 1 cm of their distal colon were extracted and fixed in 4% paraformaldehyde (PFA) for 48 h, and cryoprotected in 30% sucrose solution (72 h). Coronal cryosections of the brains were sliced at 12 μm thickness and transverse sections of the colon were sliced at 8 μm thickness. These were then mounted on super-frost slides (Thermo scientific). For immunofluorescence, the mounted tissue sections were incubated in a blocking buffer (0.2% Triton X-100, 0.05% sodium azide, 4% bovine serum albumin in PBS) for 2 h at room temperature. Primary antibodies diluted in blocking buffer were added to the desired concentration and the slides were incubated at 4°C overnight. The following primary antibodies were used for brain sections: mouse anti-NeuN (1:400, Sigma-Aldrich), rabbit anti-GFAP (1:250, Agilent), Chicken anti-GFAP (1:1000, abcam), chicken anti-mCherry (1:500, abcam) or rat anti-CD11b (1:250, BioLegend). To evaluate c-Fos expression in the brain, mice were sacrificed 90 min after CNO injection and treated as described above. Fixed sections were incubated with anti-c-Fos antibody (1:2000, abcam). The sections of the colon were incubated with a rat anti-CD45 (1:250, BioLegend), rabbit anti-ZO1 (1:250, abcam), biotin-rat anti Ep-CAM (1:250, BioLegend), or rabbit anti-lysozyme (1:250, abcam). Following overnight incubation with primary antibody, slides were then washed in PBS 3 times for 15 min, and further incubated for 60 min at room temperature with a fluorescent-conjugated secondary antibody. The following secondary antibodies were used: Alexa Fluor 488-donkey anti-mouse IgG (1:500, Jackson ImmunoResearch laboratories); Cy5 goat anti-rabbit IgG (1:300, Jackson ImmunoResearch laboratories); Cy5 goat anti-rat IgG (1:300, Jackson ImmunoResearch laboratories); Alexa Fluor-568 goat anti-chicken (1:300, Invitrogen); Alexa Fluor-488 donkey anti-chicken IgG (1:500, Jackson ImmunoResearch laboratories); and Alexa Fluor-568 goat anti-rat IgG (1:300, Invitrogen). Slides were then washed in PBS 3 times for 15 min, mounted with DAPI-mounting medium (SouthernBiotech) and covered with a glass coverslip (Bar-Naor). All images were taken at 10 × or 20 × magnification using an Axio imager M2 microscope (Carl Zeiss Inc. US).

Retrograde PRV tracing

PRV injections

Mice were anesthetized with a ketamine-xylazine mixture (ketamine 80 mg per kg body weight (mg/kg); xylazine 15-20 mg/kg; Sigma-Aldrich) in sterile saline (0.9% NaCl). Injections of Pseudorabies virus Bartha strain 152 (PRV-152 (GFP), a gift from O. Kobiler) to the colon and peritoneum were performed by adaptation of the procedure previously described by Muller et al. (2020). After shaving and sterilization of the abdomen, mice were placed on a sterile surgical pad on top of a heating pad. Ophthalmic ointment (Duratears, Alcon) was placed over the eyes to prevent dehydration and the incision site was sterilized. Upon loss of recoil paw compression, a midline incision was made through the abdominal wall, exposing the peritoneal cavity. For injection to the colon wall, colon was located, exposed for injection and held in place using two stabilized swabs. For injection to the peritoneal wall, the peritoneal wall was folded and held in place using a needle holder. We injected an overall 2 μL of virus with 0.1% FastGreen (Sigma-Aldrich) using a pulled glass micropipette placed in a 5 μL syringe (Hamilton) and a Stoelting Quintessential Stereotaxic Injector (QSI), into five different locations along the exposed tissue. Following injection, the abdominal wall and the skin were separately closed using absorbable sutures. Antibiotic ointment was applied to the closed surgical site and mice were given 0.05 mg/kg buprenorphine every 12 h for three days. Colons, peritoneal wall and brains were collected 7 d (for colon) or 6 d (for peritoneum) after injection.

Fos^{TRAP2}-PRV labeling

Fos^{TRAP2} mice were stereotactically injected with AAV8-hSyn-DIO-mCherry (for colitis experiments) or AAV1-EF1α-DIO-tdTomato (for peritonitis experiments) into their InsCtx as described above. Upon recovery from the procedure, mice were administered TM injection i.p., to induce expression of the injection viral vector in recently activated neurons. For colon-injected mice, TM was injected 48 h into 3% DSS treatment, and for peritoneum-injected mice, TM was applied 2 h before Zymosan administration. After four weeks, we injected PRV–152 with 0.1% FastGreen into the proximal colon wall or peritoneal wall (as described in the previous section). Seven or six days later (for colon or peritoneal analysis, respectively), the colons, peritoneum and brains were collected for immunofluorescence analysis.

Tissue processing

Colon, peritoneum and brains were fixed in 4% paraformaldehyde (PFA) for 48 h, and cryoprotected in 30% sucrose solution (72 h). Coronal cryosections of the brains were sliced at 12 μm thickness and sections of the colon and peritoneum were sliced at 8 μm thickness. For PRV immunofluorescence staining, the cryosections were treated as described in the previous section. Colon and peritoneum sections were stained with chicken anti-GFP (1:500, abcam), rabbit anti-β3 tubulin (1:500, abcam) and the secondary antibodies Alexa Fluor-488 donkey anti-chicken IgG (1:500, Jackson ImmunoResearch laboratories) and Alexa Fluor-568 donkey anti-rabbit IgG (1:300, Invitrogen). Brain sections were stained with the primary chicken anti-GFP (1:500, abcam) and the secondary Alexa Fluor-488 donkey anti-chicken IgG (1:500, Jackson ImmunoResearch laboratories).

Histopathological scoring of colon sections

For histology staining, mice were sacrificed, and their colons were fixed in 4% paraformaldehyde (PFA) in PBS for 48 h, cryoprotected in 30% sucrose solution for another 48 h, and then frozen on dry ice. The colons were sliced in 8 mM sections and were mounted on super-frost slides (Thermo scientific). The slides were stained with Hematoxylin & Eosin (H&E). All images were taken using an automatic slide scanner (250 Flash III). The histological scoring was then performed by an investigator blinded to the treatment group of each sample. The components of the histological score were inflammatory infiltrate, goblet cell loss, crypt density, crypt hyperplasia, muscle thickening, submucosal inflammation, crypt abscess, and ulceration (as previously described in Koelink et al., 2018).

Clinical scoring of colitis severity

Clinical severity of colitis was evaluated by monitoring the mice's body weight throughout DSS administration, and assessing stool consistency, hematochezia and colon length at the day of euthanasia. Disease activity index score was quantified for mice in the InsCtx inhibition experiments (Figure S8) by an experimenter blinded to the experimental groups, based on the sum score of weight loss, stool consistency and presence of blood in stool (as previously described (Park et al., 2015)).

smFISH

Single molecule fluorescence *in situ* hybridization (smFISH) probes were designed using the Stellaris probe designer for *GAD67* and *SLC17A7* genes conjugated with Quasar670® fluorophore (Biosearch Technologies). The procedure was obtained using the manufacturer instructions for fresh frozen mouse brain tissue with minor adjustments. Brain cryosections (12 μm) were kept at −80°C until further procedures. Slides were fixed for 15 min in cold 4% PFA in PBS following PBS wash for 5 min twice. After being dipped in nuclease-free water and 3 min incubation in 2X saline-sodium citrate (SSC) buffer, slides were immersed in serial 3 min incubations in 70%, 95%, 100% ethanol and then 5 min of chloroform incubation. Then slides were immersed in 100% followed by 95% ethanol for 3 min each, and air-dried for 60-90 minutes.

Probes were diluted in Stellarris to a concentration of 250nM (*Slc17a7*) or 375nM (*GAD67*). Slides were then covered with hybridization buffer and kept in the dark at 37°C in a humidified chamber overnight. After incubation, slides were washed in Stellaris wash buffer A for 30 min in the dark and stained with DAPI (5 ng/ml in water) for 30 min in the dark, at room temperature. Slides were then washed for 3 min in Stellaris wash buffer B and then immersed in 50%, 85%, 100% ethanol for 3 minutes each. Slides were dried and mounted.

iDISCO sample processing

Whole brain clearing was performed following the iDISCO method as previously described (Renier et al., 2014) and updated at https://www.idisco.info/. Briefly, after methanol dehydration, the brains were incubated with 5% H2O2 in methanol (MeOH) at 4°C overnight, followed by several washes in 100% methanol for 1 h. Samples were then incubated in a 66% dichloromethane (DCM, Bio-Lab) and 33% MeOH solution at room temperature, and then in 100% DCM for 15 min twice, while shaking (to rinse out any remaining MeOH). Tissues were stored in refractive index (RI) matching solution (RI = 1.56), Dibenzyl ether (DBE, Sigma-Aldrich) until imaging.

Light-sheet imaging

Whole-brain cleared samples were imaged while submerged in dibenzyl ether in a Light Sheet Fluorescent Microscope (LSFM, Lightsheet 7, Zeiss), using a 561 nm light-sheet illumination, a 5 × / 0.16 foc objective and 5 μm z-slices.

Flow cytometry

Mice were euthanized, and their blood, mesenteric lymph nodes (mLN), peritoneal lavage fluid (PLF) and colon (starting at the cecocolic junction proximally and ending at the anus distally) were collected. EDTA-coated tubes were used for blood collection, and centrifuged at 1200 rpm for 10 min. For blood cell analysis, 1 mL of blood was incubated with 9 mL of RBC Lysis buffer (BD biosciences) for 15 min and washed twice with PBS. mLN were dissociated in PBS into single-cell suspensions and mesh-filtered (40 μm) to remove fat tissue and debris. Peritoneal cells were collected via peritoneal lavage; 6 mL of cold PBS was carefully injected into the peritoneum and the cell-containing fluid was collected with a Pasteur pipette into 15 mL tubes. These were centrifuged at 1200 rpm for 5 min. PLF supernatant was extracted and frozen at −20°C for further protein analysis. The recovered cells were incubated for 3 min with 1 mL of Lysis buffer and washed once with PBS. In case of blood-contamination in PLF samples, these samples were excluded from the experiment. Colon tissue was mechanically dissociated into intraepithelial lymphocytes (IEL) and enzymatically dissociated into lamina propria (LP) single-cell suspensions using the Lamina propria dissociation kit (Miltenyi Biotec) and a GentelMacs Dissociator (Miltenyi Biotec). For viability staining, cells (10^6) were washed once with PBS, resuspended in Zombie Aqua™ dye solution (1:1,000, BioLegend) and incubated in the dark for 15 min at room temperature. For extracellular staining, cells were washed with FACS staining buffer (PBS containing 1% bovine serum albumin, 1 mM EDTA and 0.05% sodium azide) and incubated with antibodies for 30 min at 4 °C. For Streptavidin-based staining, following extracellular staining, samples were washed twice and incubated for 25 min at 4 °C with fluorescently-conjugated streptavidin diluted to the desired concentration in FACS staining buffer. For intracellular staining, the samples were first stained for extracellular markers as described above, fixed and permeabilized with BD Cytofix/Cytoperm kit, and stained with the intracellular antibodies. The following mAbs were used (from Biolegend, San Diego, CA, US unless stated otherwise): Alexa Fluor-700 anti-CD45, Alexa Fluor-647 anti-TLR2, Biotin anti-TLR4 and Biotin anti-IL-12/IL-23, Biotin and Brilliant violet 650 anti-CD69, PE/Cy7 anti-IFN-γ, PerCP/Cy5.5 anti-CD11b, APC and APC/Cy7 anti-F4/80, FITC and Alexa Fluor 700 anti-Ly6G, Brilliant violet 510 anti-Gr-1, Brilliant violet 510 and FITC anti-Ly6C, PerCP and Alexa fluor 488 anti-CD8, APC and PE/Dazzle 594 anti CD4, PE/Cy7 and PE/Dazzle 594 anti-CD11c, Alexa Fluor-488 and Pacific blue anti-I-A/I-E, PE anti-TCRγδ, APC anti-TCRγδ, Pacific-blue anti-TCRβ, PE/Cy7 anti-CD25, Brilliant violet 605 anti-CD62L, Brilliant violet 510 anti-CD44, Brilliant-violet-605 anti-CD103, PE/Cy7 anti-CD19, Alexa Fluor 488-conjugated streptavidin (Jackson), Brilliant violet 605-conjugated streptavidin, FITC anti-TNFα, PE/Cy7 anti-IL-2, PerCP/Cy5.5 anti-IL-22, PE anti-IL-6, PE anti-IL-13 and Brilliant violet 510 anti-IL-17. All antibodies were validated by the manufacturers for flow application, as indicated on the manufacturers' websites. After the incubation of the samples with the antibodies, the samples were washed twice with FACS staining buffer and re-suspended in 250 μl of 1% PFA. Samples were analyzed with a CytoFLEX S cell analyzer and FlowJo software. For visualization of the immune cell subsets that were analyzed, flow cytometry dataset was subjected to the unsupervised identification method, FlowSOM (Gassen et al., 2015). Briefly, we concatenated an equal number of live $CD45^+$ cells from IEL and LP tissues or PLF to generate a single FlowSOM tree.

Measurement of cytokine levels

For peritoneal lavage fluid (PLF) protein analysis, 6 mL of cold PBS were carefully injected into the peritoneum and the cell-containing fluid was collected with a Pasteur pipette into 15 mL tubes. These were centrifuged at 1200 rpm for 5 min. PLF supernatant was extracted and frozen at −20°C for further protein analysis. For colon protein analysis, a 200 mg piece of the tissue was collected from each mouse. These samples were homogenized in a PBS (1 mg: 2 μl) using stainless steel beads and the Bullet Blender Storm 24 (Next Advance), according to the recommended protocol at the manufacturer's website (nextadvance.com). PLF supernatant and homogenized colon samples were analyzed using standard ELISA kits for TNF-α, IL-6, IL-17 and IL-10 (PeproTech).

Corticosterone and Noradrenaline measurement

Mice were euthanized, and their blood was collected into EDTA-coated tubes. These were then centrifuged at 1200 rpm for 10 min, and plasma was collected and frozen at −20°C until further analysis. On the day of analysis, samples were thawed and corticosterone and noradrenaline concentrations were measured in plasma, using the corticosterone (Enzo) and noradrenaline (IBL-America) ELISA kits.

Von Frey test

Abdominal pain sensitivity was measured using Von Frey filaments as previously described (Jain et al., 2020). In brief, mice were randomly divided into 3 groups: 2 that were injected with Zymosan and 1 with PBS. 24 h later, one Zymosan-injected group received an Acetaminophen i.p. injection (300 mg/kg), and the other two groups received saline as a control for the analgesia. We chose Acetaminophen because it has relatively low anti-inflammatory effects (although it may have a direct effect on Kupffer cells), and it does not block the transition of neuronal inputs to the brain (Jóźwiak-Bebenista and Nowak, 2014).10 min later, mice were habituated in metal cubic compartments (13x15 cm^2) with a mesh bottom for 15 min. A blinded observer applied Von Frey filaments to the abdomen in ascending order starting at 0.02, 0.04, 0.07, 0.16, 0.4, and 0.6 g forces followed by the same descending order. Each filament was applied three times with maximal duration of 2-3 s, and a 5 s interval between each poke. The number of withdrawal responses (licking, retraction, or abdomen withdrawal) was quantified and summed for each mouse.

Illustrations

The graphical abstract was created with BioRender.com. All figures were created using Illustrator software (Adobe).

QUANTIFICATION AND STATISTICAL ANALYSIS

Statistical details for every experiment are provided in the figure legends, where *n* represents the number of animals per group (unless stated otherwise). Statistical significance was defined as $p < 0.05$. Sample size was chosen based on calibration experiments to detect statistical significance under technical feasibility constrains.

Quantification

Brain sections analysis

Following immunofluorescence staining or smFISH, positive or double-positive cells for c-Fos, AAV (mCherry or GFP) PRV, GFAP, CD11b, NeuN, vGlut1 and GAD67 were counted manually using the ImageJ (fiji) Software (Schindelin et al., 2012).

Colon sections analysis

Following immunofluorescence staining, analysis was performed using ImageJ (fiji) Software in a double-blinded manner. Images were pre-processed manually by subtracting each image background intensity, as measured at a blank area in the same frame. Quantification was achieved by manually defining the region of interest (ROI) based on the tissue morphology: epithelium area for ZO-1 and EpCAM; mucosa for $CD45^+$ cells; or colon crypts for lysozyme, and calculating mean intensities for all ROIs.

Cleared brain analysis

Quantification of the difference in TRAPed $tdTomato^+$ neurons in cleared whole-brains of inflamed and non-inflamed mice was performed by adapting the ClearMap pipeline (Renier et al., 2016), in which intensity for each brain area was compared between the two experimental groups.

Statistical analysis

In all experiments, significance levels of the data were determined using GraphPad PRISM 9.0.0 (121). We used two-tailed unpaired or paired Student's t test when comparing two independent or dependent groups, respectively. For the comparison between more than two groups, we used one-way ANOVA if there was a single independent variable or two-way ANOVA for two-factorial designs (e.g., brain region x group). To further test pairwise differences between groups we used Tukey's, Šídák's or Benjamini, Krieger and Yekutieli Multiple comparisons tests (as specifically mentioned for every experiment in the figures legend). Data are represented as mean ± standard error of mean (s.e.m) or as median ± min/ max in the box and whiskers graphs (as stated in figure legends). Outliers were excluded using ROUT method for outlier identification (Motulsky and Brown, 2006) with a False Discovery Rate less than 1% ($Q < 1\%$). All experiments were performed at least twice.

CellPress

Supplemental figures

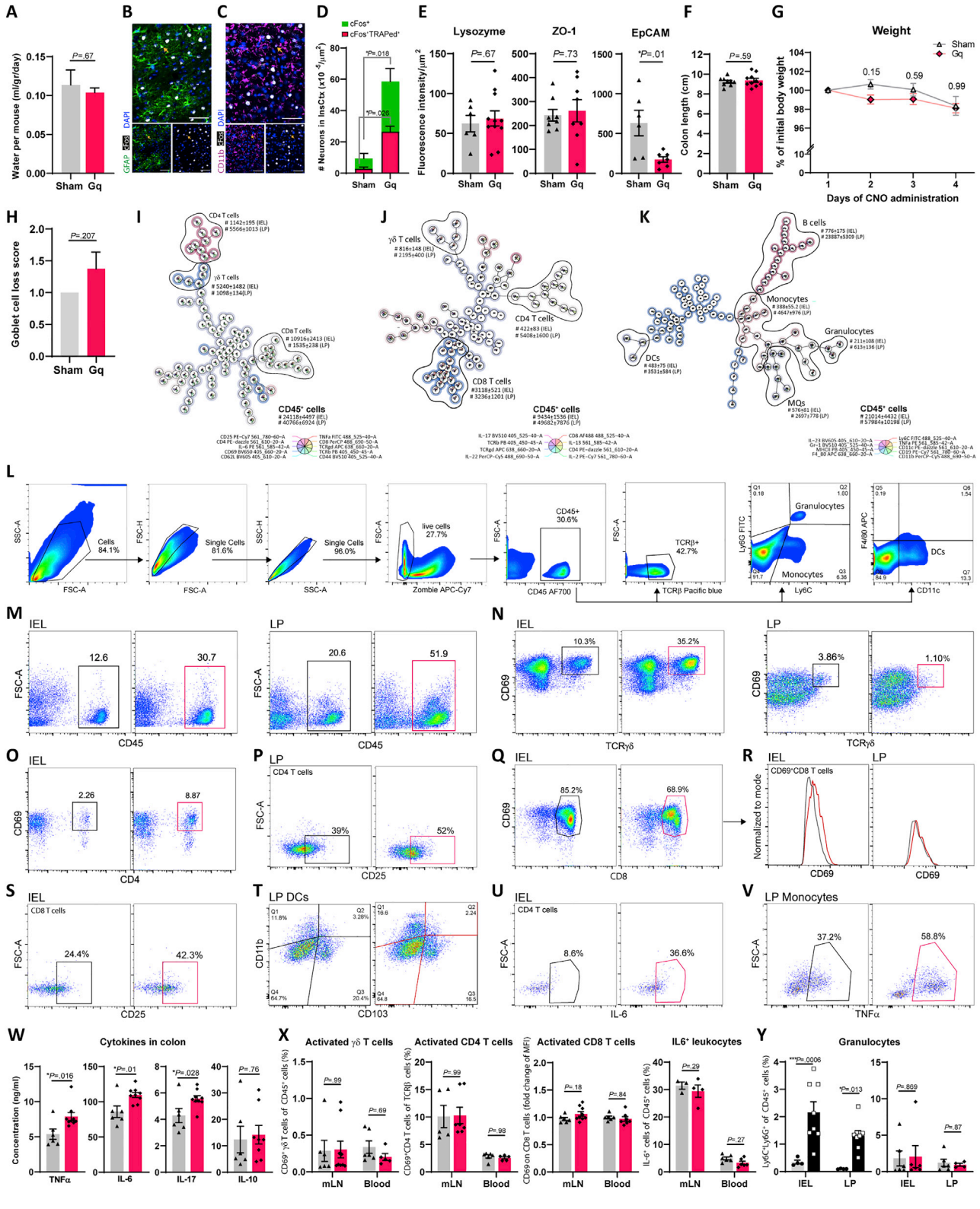

(legend on next page)

Figure S1. Immunological, neuronal, and clinical analysis following reactivation of InsCtx neurons captured during colitis, related to Figure 2

(A) Quantification of water consumed by Gq mice compared to their sham control mice throughout the 4 d of InsCtx reactivation (CNO administration). Student's t test (*n* cages = 2, 2). (B-C) Representative micrographs demonstrating IF staining of cFos$^+$ (white) and (B) astrocytes (GFAP$^+$, green) or (C) microglia (CD11b$^+$, magenta). Orange arrows indicate double-stained cells for cFos$^+$ and the relevant glial marker (n = 3). Scale bars: 50 μm. (D) Quantification of cFos$^+$ and cFos$^+$TRAPed$^+$ cells in the InsCtx (IF-stained brain sections) of Gq mice and their sham controls, 90 min following CNO administration. Šídák's multiple comparisons test (n = 3, 4). (E) Assessment of Paneth cells and gut permeability based on IF-staining of colon sections for lysozyme, and ZO-1 and EpCAM, respectively. Student's t test. (F) Colon length measurements of Gq mice and their sham controls after 4 d of daily CNO administration. Student's t test. (G) Body weight measurements of Gq and their sham controls mice during InsCtx reactivation. Šídák's multiple comparisons test (n = 9, 10). (H) Goblet cell loss score of H&E stained colons of Gq mice and their sham controls after 4 d of daily CNO administration. Student's t test (n = 7, 8). (I-K) FlowSOM graphs presenting the extra- and intra-cellular immune markers of colonic IEL and LP cells identified by flow cytometry analysis for the specific markers indicated in the pie chart. Numbers of cells analyzed are presented as mean ± s.e.m. Total number of analyzed cells from each population is indicated. (L) Gating strategy of the different immune cell subpopulations in the colon mucosal layer analyzed by flow cytometry and presented in Figures 2E–2O. (M-V) Representative dot plots of the immunological effects induced by InsCtx reactivation, as shown in Figures 2E–2O. These include (M) mucosal leukocytes (CD45$^+$ cells), (N) activated γδ T cells, (O, P) activated CD4 T cells, (Q-S) activated CD8 T cells, (T) dendritic cells, (U) IL-6$^+$ CD4 T cells, and (V) monocytes from the colon of Gq-mice and their sham controls (gated in red and black, respectively). (W) Graphs derived from cytokine ELISA showing concentrations of TNFα, IL-6, IL-17, and IL-10 in colons of the Gq group compared to its sham viral vector controls. Student's t test. One sample was excluded from the data (IL-10); ROUT method for outlier detection (Q = 1%). (X) Graphs showing percentages of (from left to right) activated γδ T cells, activated CD4$^+$ T cells, CD69 expression (fold change of MFI) on CD8$^+$ T cells, and percentages of IL-6$^+$ leukocytes from mesenteric lymph nodes (mLN) and peripheral blood, of Gq mice relative to their sham viral vector controls following neuronal reactivation. Student's t tests. (Y) Graphs derived from flow cytometry analysis showing percentages of granulocytes in the colonic mucosal layer (IEL, LP) of DSS+ mice and their non-inflamed controls (left) and Gq mice relative to their sham controls following neuronal reactivation (right). Student's t tests. In (A, D-H, W-Y) graphs, data are represented as mean ± s.e.m. Experimental groups are depicted in Figure 2A. InsCtx, insular cortex; IEL, intraepithelial lymphocytes; LP, lamina propria; DCs, dendritic cells; MQs, macrophages; MFI, median fluorescence intensity; IF, immunofluorescence. Data represent two independent repeats.

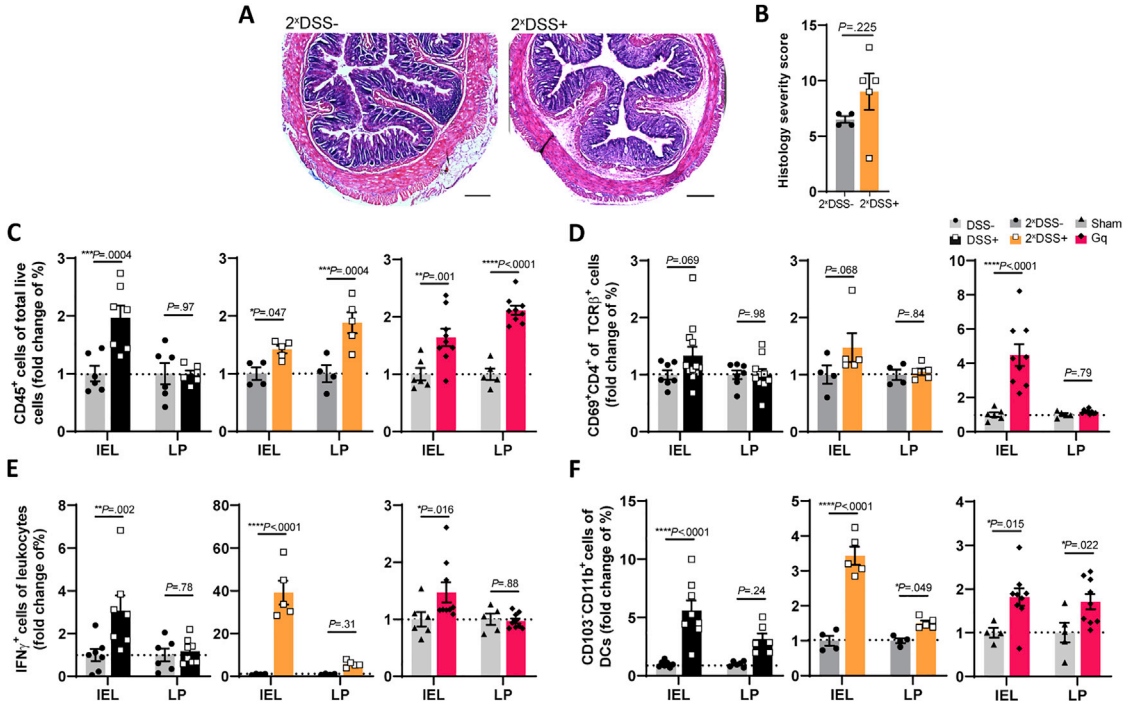

Figure S2. Comparison between immune characteristics induced by DSS administration alone or reactivation of InsCtx neuronal ensembles captured during colitis, related to Figure 2

(A) C57BL/6J WT mice received 3% DSS in their drinking water for 84 h, corresponding to the DSS-induced colitis elicited in *Fos*^{TRAP} mice during neuronal labeling. 4 w later, one group received a second dose of 3% DSS for 4 days (2ˣDSS+) and a second group received normal drinking water as controls (2ˣDSS-), corresponding to the 4 d of CNO administration in *Fos*^{TRAP} mice during InsCtx reactivation. Presented are micrographs of colon sections from both groups stained with H&E. Scale bar: 200 μm. (B) Histological severity score of H&E stained colon sections. Student's t test. (C-F) Graphs derived from flow cytometry analysis comparing immunological effects of 3 experiments: 1. A single DSS-induced colitis model (3% DSS water for 84 h); 2. A second exposure to DSS (as described above, in A); 3. The InsCtx reactivation experiment (as schemed in Figure 2A). Shown here is fold change of (C) percentages of leukocytes, (D) activated CD4$^+$ T cells, (E) IFNγ^+ leukocytes, and (F) CD103$^-$CD11b$^+$ DCs in the colonic mucosal layer (IEL and LP). Student's t test. DSS, dextran sulfate sodium; IEL, intraepithelial lymphocytes; LP, lamina propria; DCs, dendritic cells. Data represent two independent repeats.

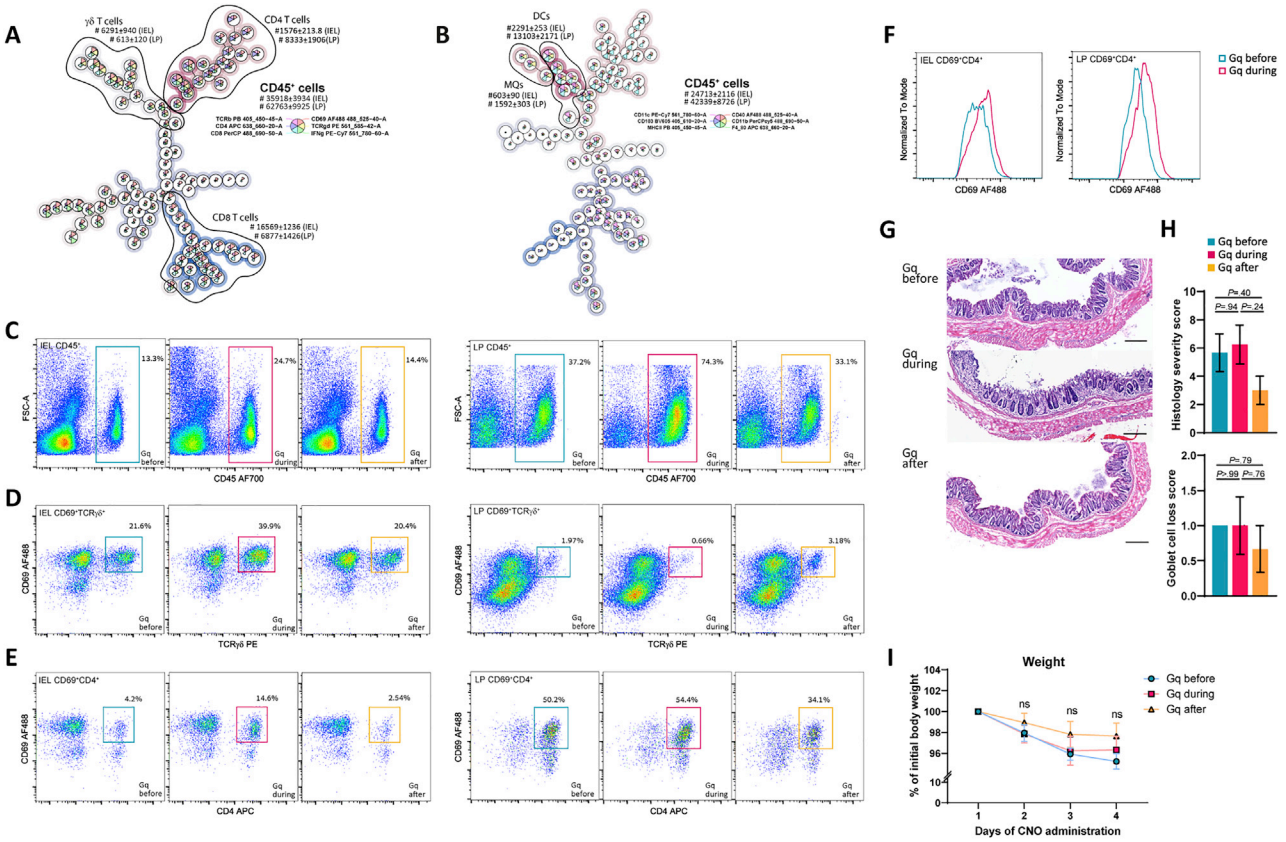

Figure S3. Immune cells in the colon following reactivation of InsCtx neuronal ensembles captured at different time points relative to colitis induction, related to Figure 3

(A-B) FlowSOM graphs presenting the extra- and intra-cellular immune markers of colonic IEL and LP cells identified by flow cytometry analysis for the specific markers indicated in the pie chart. Numbers of cells analyzed are presented as mean ± s.e.m. Total number of analyzed cells from each population is indicated. (C-E) Representative dot plots of (C) mucosal leukocytes (CD45$^+$ cells), (D) activated γδ T cells and (E) activated CD4 T cells from IEL and LP of the Gq before, during and after groups (gated in blue, red and orange, respectively). (F) Representative histograms of CD69 expression level (MFI) on activated CD4 T cells from IEL and LP of Gq before (blue) layered against histograms of the Gq-during group (red). (G) Micrographs of colon sections stained with H&E, from the three experimental groups. Scale bar: 200 μm. n = 3, 4, 3. (H) Histological severity score and goblet cell loss score of H&E stained colon sections. One-way ANOVA and Tukey's multiple comparison test (n = 3, 4, 3). (I) Body weight measurements of all three experimental groups during the 4 d of CNO administration. Benjamini, Krieger and Yekutieli Multiple comparisons (n = 4, 4, 7). In (H-I) data are represented as mean ± s.e.m. Experimental groups are depicted in Figure 3A. InsCtx, insular cortex; IEL, intraepithelial lymphocytes; LP, lamina propria; MFI, median fluorescence intensity; ns, non-significant.

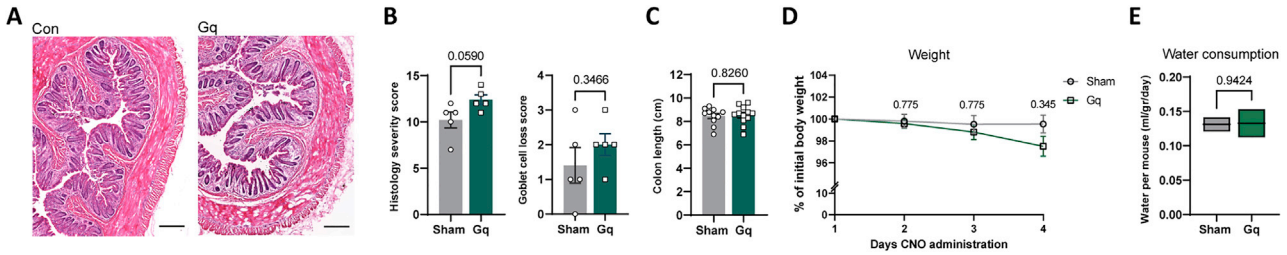

Figure S4. Histological and clinical evaluation following non-specific InsCtx activation in mice with prior DSS exposure, related to Figure 4

(A) Representative micrographs of colon sections stained with H&E, from Gq mice and their sham controls (as depicted in Figure 4L). Scale bar: 200 μm. n = 5, 5. (B) Histological severity score (left) and goblet cell loss score (right) of H&E stained colon sections. Student's t test. (C) Colon length measurements of Gq mice and their sham controls after 4 d of daily CNO administration. Student's t test. (D) Weight measurements of mice from the two experimental groups during the 4 d of CNO administration. Benjamini, Krieger and Yekutieli Multiple comparisons (n = 8, 8). In (B-D) graphs, data from individual mice are shown, and values are represented as mean ± s.e.m. (E) Averaged consumption of water by Gq mice compared to their sham control mice during the 4 d of InsCtx reactivation (CNO administration). Student's t test (*n* cages = 2, 2). Data are represented as median + min/max. Experimental groups are depicted in Figure 4L. InsCtx, insular cortex. Data represent two independent repeats.

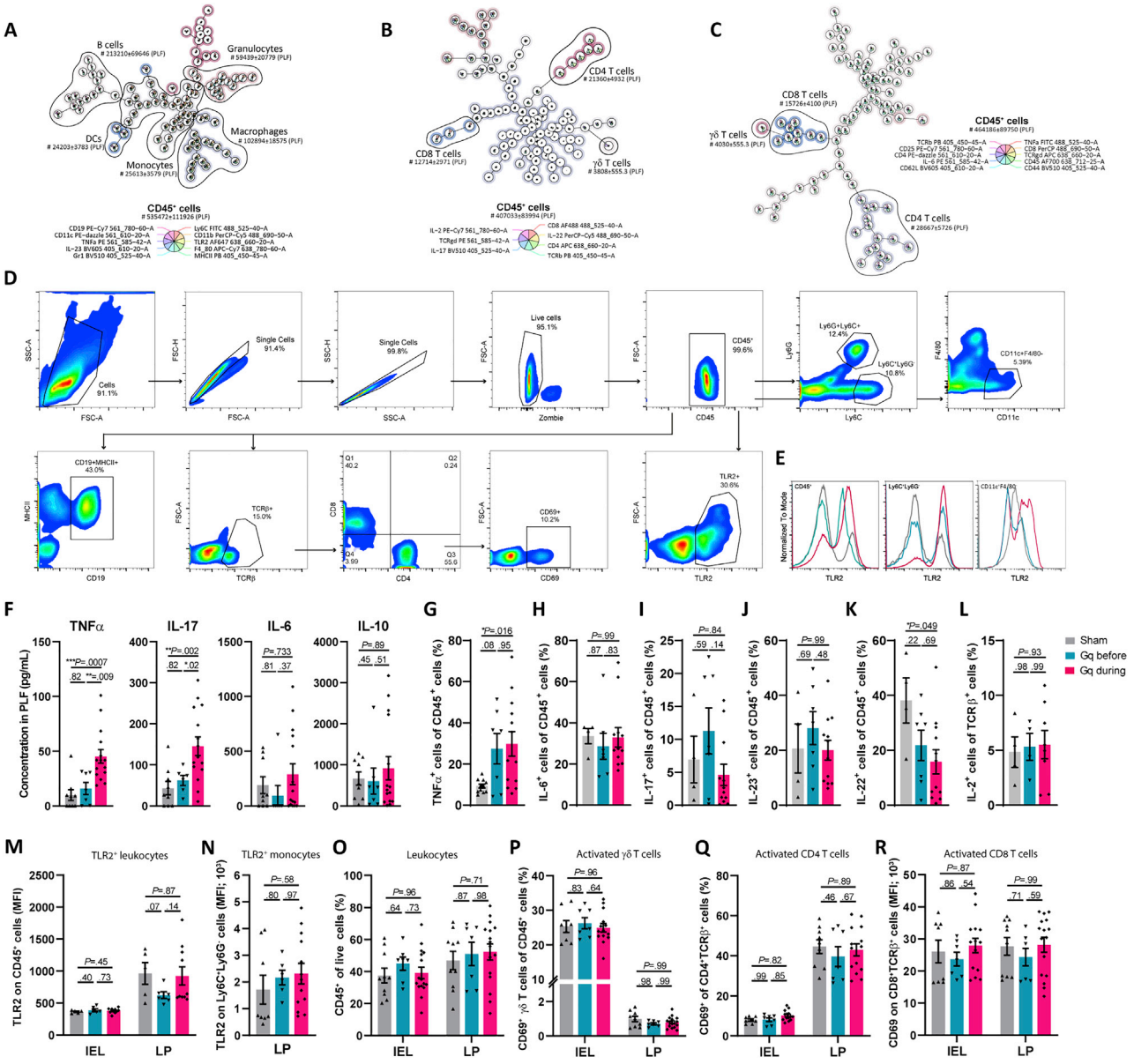

Figure S5. Immunological and neuronal analysis following reactivation of InsCtx neurons captured during peritonitis, related to Figure 5

(A-C) FlowSOM graphs presenting the extra- and intra-cellular immune markers of PLF cells identified by flow cytometry analysis for the specific markers indicated in the pie chart. Numbers of cells analyzed are presented as mean ± s.e.m. Total number of analyzed cells from each population is indicated. (D) Gating strategy of the immune cell subpopulations analyzed by flow cytometry and presented in Figures 5D–5O. (E) Representative histograms of TLR2 expression (MFI) on leukocytes (CD45$^+$ cells), monocytes (Ly6C$^+$Ly6G$^-$) and DCs (CD11c$^+$F4/80$^-$). (F) Graphs derived from cytokine ELISA showing concentrations of TNFα, IL-17, IL-6, and IL-10 in PLF of the Gq groups compared to their sham viral vector controls. One-way ANOVA and Tukey's multiple comparison test. One sample (IL-17) was excluded from the data; ROUT method for outlier detection (Q = 1%). (G-L) Graphs derived from flow cytometry analysis of (G) TNFα$^+$, (H) IL-6$^+$, (I) IL-17$^+$, (J) IL-23$^+$, (K) IL-22$^+$ leukocytes and (L) IL-2$^+$ T cells in PLF of the Gq groups compared to their sham viral vector controls. (M-R) Graphs derived from flow cytometry analysis showing (M) TLR2 expression (MFI) on IEL and LP leukocytes and (N) LP monocytes, and (O) percentages of colonic leukocytes, (P) activated γδ T cells, (Q) activated CD4$^+$ T cells, and (R) CD69 expression (MFI) on CD8$^+$ T cells of the two Gq groups and their sham viral vector controls. (F-R) One-way ANOVA and Tukey's multiple comparisons test. In all bar graphs, data from individual mice are shown, and values are represented as mean ± s.e.m. DCs, dendritic cells; MQs, macrophages; InsCtx, insular cortex; TM, Tamoxifen; PLF, Peritoneal lavage fluid; MFI, median fluorescence intensity; ZIP, Zymosan-induced peritonitis; IEL, intraepithelial lymphocytes; LP, lamina propria. Data represent two independent repeats.

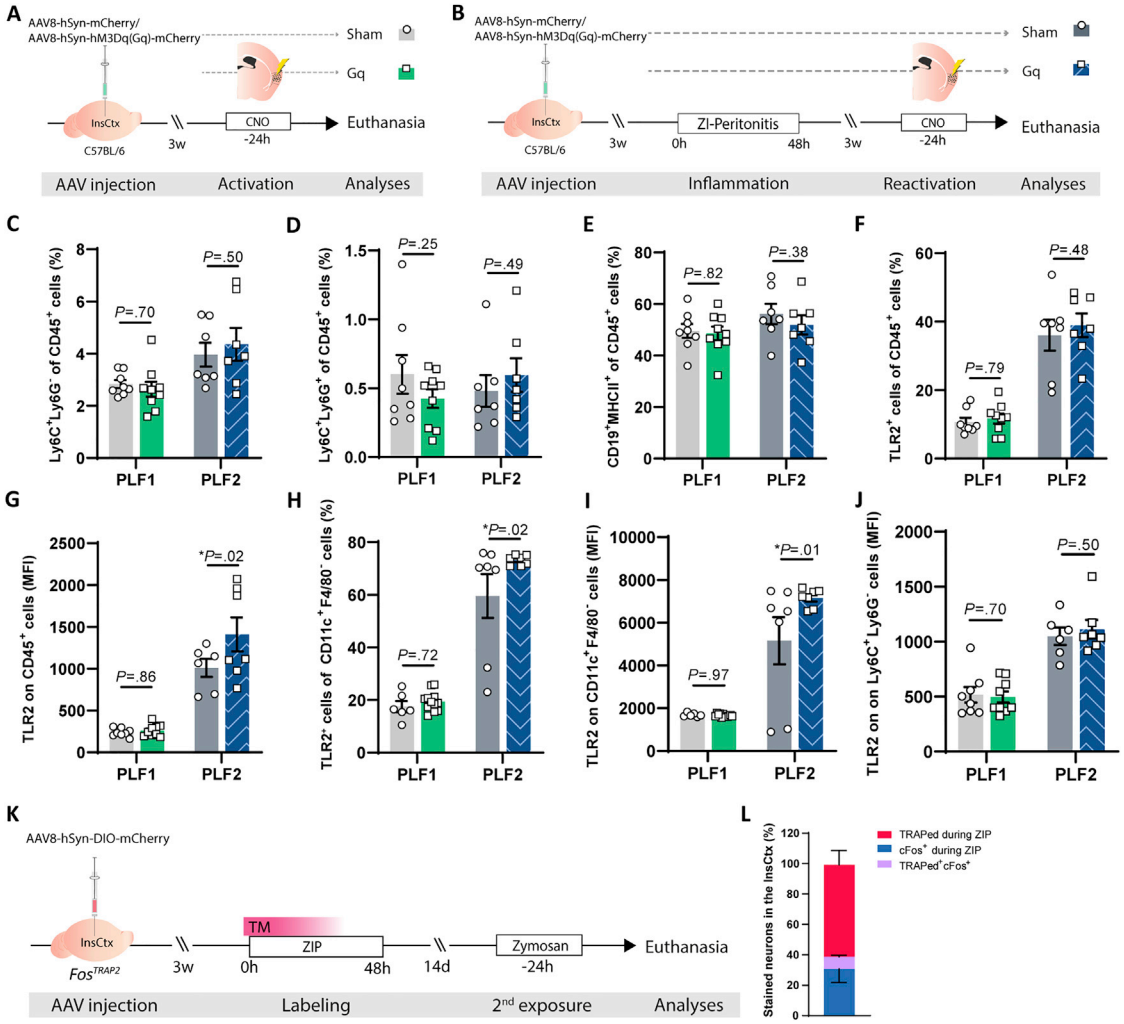

Figure S6. Immunological effects in the peritoneum following non-specific activation of the InsCtx after a prior exposure to zymosan-induced peritonitis, related to Figure 5

(A) Schematic representation of viral vector expression in InsCtx neurons in a nonspecific manner (Cre-independent) in C57BL/6 WT mice. One group was stereotactically injected with a Gq-DREADD and a second group with a sham viral vector as controls. Three weeks after stereotactic injections, all mice received a single injection of CNO, and the immune response was analyzed 24 h later. (B) Schematic representation of viral vector expression in InsCtx neurons in a nonspecific manner (Cre-independent) in C57BL/6 WT mice. One group was stereotactically injected with a Gq-DREADD and a second group with a sham viral vector as controls. Three weeks after stereotactic injections, all mice were administered with Zymosan, followed by a single CNO injection 4 weeks later. (C-J) Graphs derived from flow cytometry analysis of the two experiments depicted in A and B (PLF1 and PLF2, respectively), showing percentages of (C) peritoneal monocytes ($Ly6C^+Ly6G^-$), (D) granulocytes ($Ly6C^+Ly6G^+$), (E) B cells ($CD19^+MHCII^+$), (F) $TLR2^+$ leukocytes, (G) expression (MFI) of TLR2 on leukocytes, percentages of (H) $TLR2^+$ DCs ($CD11c^+F4/80^-$) and expression (MFI) of TLR2 on (I) DCs and (J) monocytes. In (C-J) Data from individual mice are shown and values are represented as mean ± s.e.m. Student's t test. (K) Schematic representation of enabling TRAPing of neuronal ensembles that were active during ZIP in the InsCtx of Fos^{TRAP2} mice. Fourteen days after neuronal labeling, mice were re-exposed to Zymosan and were euthanized after 24h for fluorescence microscopy analysis. (L) Quantification of neurons in the InsCtx that were TRAPed during ZIP and $cFos^+$ as a marker for neuronal activity following a 2nd Zymosan administration (n = 3). InsCtx, insular cortex; WT, wild-type; PLF, Peritoneal lavage fluid; DCs, dendritic cells; MFI, median fluorescence intensity; ZIP, Zymosan-induced peritonitis; Zym, Zymosan. Data represent two independent repeats.

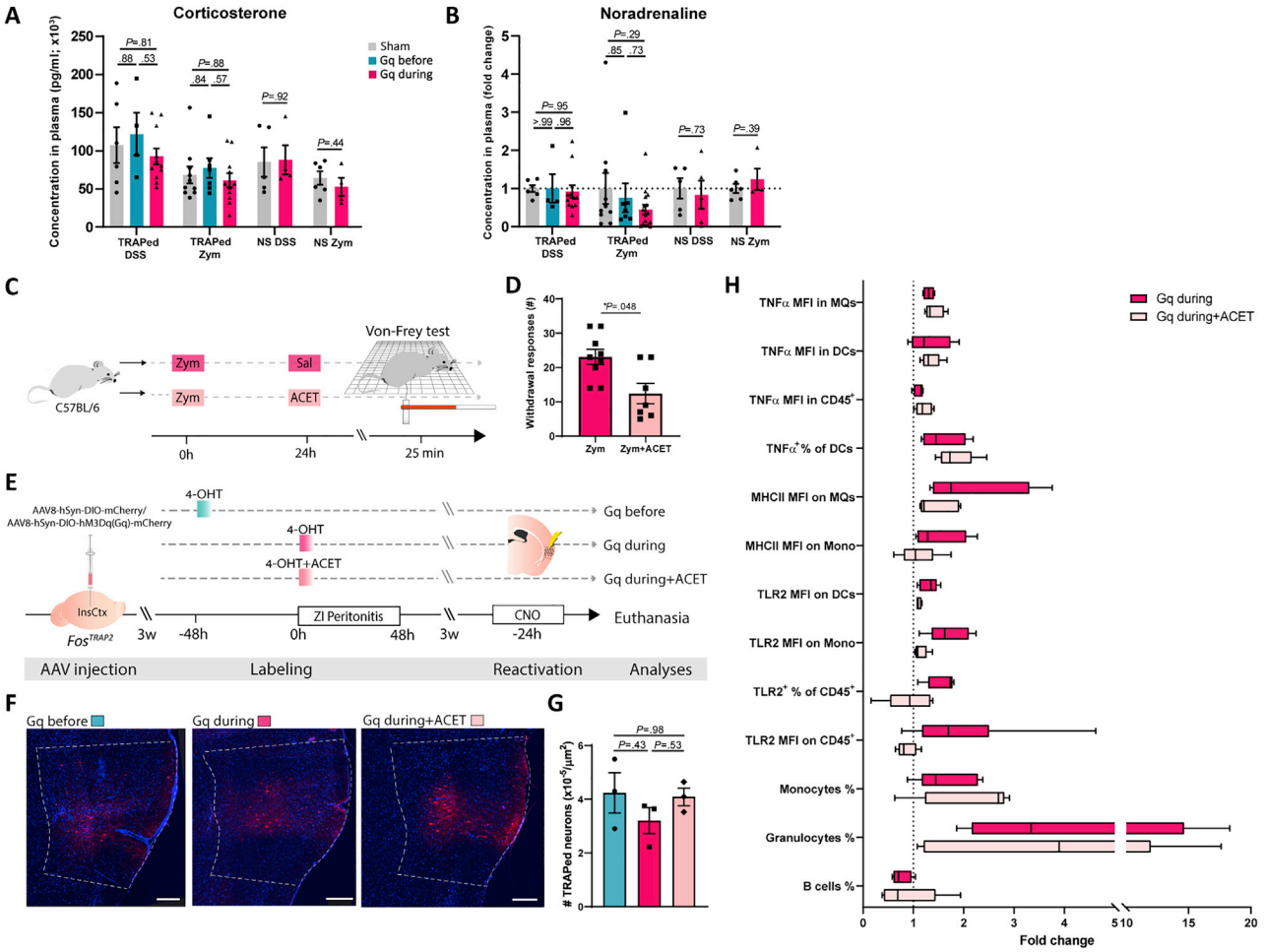

Figure S7. The involvement of stress and pain in the immunological effects induced by InsCtx activation, related to Figure 5

(A) Corticosterone and (B) Noradrenaline levels in the plasma of mice from four independent InsCtx activation experiments: 1. TRAPed DSS (Figure 3A); 2. TRAPed Zym (Figure 5A); 3. NS DSS (Figure 4L) and 4. NS Zym (Figure S6B). Tukey's multiple comparisons and Student's t test. NS, non-specific. (C) Schematic representation of the Von-Frey test for visceral pain assessment 24h following Zymosan administration, with administration of ACET or saline as controls. (D) Sum of withdrawal responses per mouse during the Von-Frey test. Student's t test. (E) Schematic representation of enabling Gq-DREADD expression in neuronal ensembles in the InsCtx of *Fos*^{TRAP2} mice. Using 4-OHT, labeling occurred before (Gq before) or during ZI-peritonitis (Gq during), or during ZI-peritonitis with analgesia (Gq during+ACET). Three weeks after Zymosan administration, all mice received a single i.p. CNO injection, and the immune response was analyzed 24h later. (F) Representative fluorescence microscopy imaging showing the expression of the injected Cre-dependent DREADD (mCherry, in red) in the InsCtx of all three experimental groups. Scale bar: 200 µm. (G) Quantification of DREADD-expressing neurons in the InsCtx of all 3 experimental groups. One-way ANOVA and Tukey's multiple comparisons test. (H) Graph derived from flow cytometry analysis of PLF extracted from the Gq-during and Gq-during+ACET mice. Data are presented as fold change of these two groups compared to the mean values of the Gq-before group (n = 4, 4, 5). InsCtx, insular cortex; ZI-peritonitis/ ZIP, Zymosan-induced peritonitis; 4-OHT, 4-Hydroxytamoxifen; CNO, clozapine-*N*-oxide; PLF, peritoneal lavage fluid; mLN, mesenteric lymph-nodes; Zym, Zymosan; ACET, Acetaminophen; MFI, median fluorescence intensity; DCs, dendritic cells; MQs, macrophages; Mono, monocytes. Data represent two independent repeats for each experimental design.

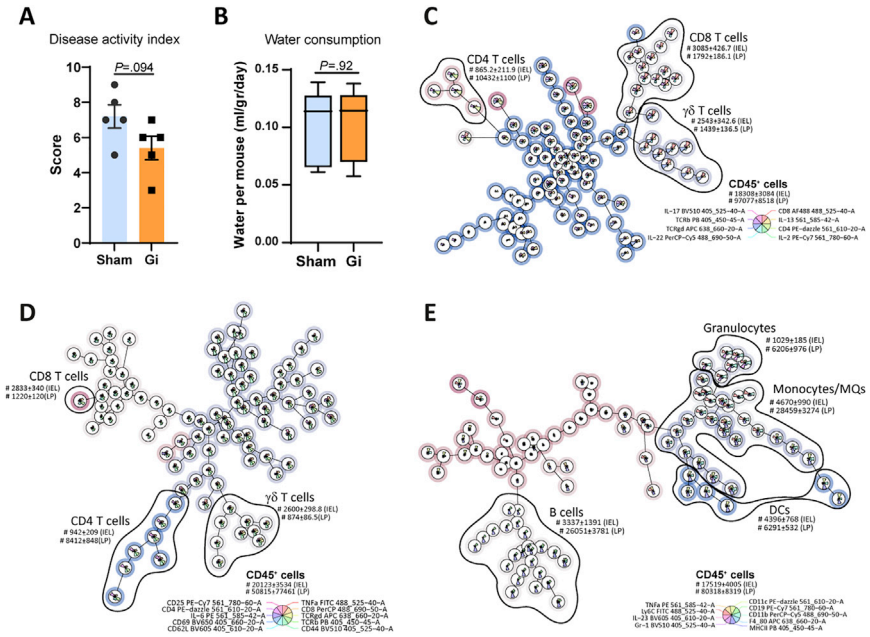

Figure S8. Immunological and clinical analysis following inhibition of the InsCtx during DSS-induced colitis, related to Figure 7

(A) Measurement of disease activity index based on weight loss, stool consistency and blood in stool in Gi mice and their sham controls, following 7d of DSS and CNO administration. Student's t test; mean ± s.e.m. (B) Averaged consumption of water by Gi mice compared to their sham control mice during the 7d of DSS administration and InsCtx inhibition (CNO administration). Student's t test; median + min/max (*n* cages = 2, 2). (C-E) FlowSOM graphs presenting the extra- and intra-cellular immune markers of colonic IEL and LP cells identified by flow cytometry analysis for the specific markers indicated in the pie chart. Numbers of cells analyzed are presented as mean ± s.e.m. Total number of analyzed cells from each population is indicated. DCs, dendritic cells; MQs, macrophages; InsCtx, insular cortex. Data represent two independent repeats.